European Journal of Pharmacology 903 (2021) 174136

Contents lists available at ScienceDirect

European Journal of Pharmacology

journal homepage: www.elsevier.com/locate/ejphar

Acteoside exerts neuroprotection effects in the model of Parkinson's disease via inducing autophagy: Network pharmacology and experimental study

Mutalifu Aimaiti [a,b,c,1], Ainiwaer Wumaier [b,1], Yiliyasi Aisa [a,b], Yu Zhang [a,d], Xirenayi Xirepu [a,e], Yilizire Aibaidula [a,f], XiuYing Lei [a,g], Qian Chen [a,g], XueZhao Feng [a,g], Na Mi [a,*]

[a] State Key Laboratory of Pathogenesis, Prevention and Treatment of Central Asian High Incidence Diseases, Clinical Medical Research Institute, The First Affiliated Hospital of Xinjiang Medical University, Urumqi, 830054, Xinjiang, China
[b] Department of Pharmacology, College of Pharmacy, Xinjiang Medical University, Urumqi, 830017, Xinjiang, China
[c] Central Laboratory, Xinjiang Medical University, Urumqi, 830011, Xinjiang, China
[d] Department of Biology, School of Basic Medical Sciences, Xinjiang Medical University, Urumqi, 830017, Xinjiang, China
[e] Department of Teaching and Research of Crude Drugs, College of Pharmacy, Xinjiang Medical University, Urumqi, 830017, Xinjiang, China
[f] Department of Pharmaceutical Analysis, College of Pharmacy, Xinjiang Medical University, Urumqi, 830017, Xinjiang, China
[g] Department of Biochemistry, College of Basic Medical Sciences, Xinjiang Medical University, Urumqi, 830017, Xinjiang, China

ARTICLE INFO

Keywords:
Acteoside
Parkinson's disease
Network pharmacology
Autophagy
Apoptosis

ABSTRACT

Parkinson's disease (PD) is the second most common neurodegenerative disease after Alzheimer's disease. At present, the incidence rate of PD is increasing worldwide, there is no effective cure available so far, and currently using drugs are still limited in efficacy due to serious side effects. Acteoside (ACT) is an active ingredient of many valuable medicinal plants, possesses potential therapeutic effects on many pathological conditions. In this study, we dissected the neuroprotection effects of ACT on PD and its potential molecular mechanism in our PD model pathology based on network pharmacology prediction and experimental assays. Network pharmacology and bioinformatics analysis demonstrated that ACT has 381 potential targets; among them 78 putative targets associated with PD were closely related to cellular autophagy and apoptotic processes. Our experimental results showed that ACT exerted significant neuroprotection effects on Rotenone (ROT) -induced injury of neuronal cells and *Drosophila melanogaster (D. melanogaster)*. Meanwhile, ACT treatment induced autophagy in both neuronal cell lines and fat bodies of *D. melanogaster*. Furthermore, ACT treatment decreased ROT induced apoptotic rate and reactive oxygen species production, increased mitochondrial membrane potentials in neuronal cells, and promoted clearance of α-synuclein (SNCA) aggregations in SNCA overexpressed cell model through the autophagy-lysosome pathway. Interestingly, ACT treatment significantly enhanced mitophagy and protected cell injury in neuronal cells. Taken together, ACT may represent a potent stimulator of mitophagy pathway, thereby exerts preventive and therapeutic effects against neurodegenerative diseases such as PD by clearing pathogenic proteins and impaired cellular organelles like damaged mitochondria in neurons.

1. Introduction

Parkinson's disease (PD) is a debilitating neurodegenerative movement disorder (Pan et al., 2019), manifests as bradykinesia, resting tremors, speech disorders, muscle rigidity, and postural instability. From 1990 to 2015, the number of people with PD globally doubled to over 6 million, this number is predicted to double again by 2040 (Dorsey et al., 2018). Neuropathologically, PD is characterized by degeneration and loss of dopaminergic neurons and intracellular accumulation of SNCA containing Lewy bodies in the substantia nigra pars compacta (Angelopoulou et al., 2019). As more than 90% PD cases are idiopathic (Hong et al., 2017), increased PD risk was closely associated with the exposure to environmental neurotoxins, e.g., 1-methyl-4-phenyl-1, 2, 3, 6-tetrahydropyridine (MPTP), paraquat, and ROT (Miller et al., 2009). As an inhibitor of mitochondrial electron transport chain complex I, ROT possesses highly lipophilic properties, is generally used to develop animal and cellular models of PD (Kadigamuwa et al., 2016; Areiza-Mazo et al., 2018; Doktór et al., 2019).

* Corresponding author.
E-mail address: mina2a@163.com (N. Mi).
[1] These authors contributed equally to this work.

https://doi.org/10.1016/j.ejphar.2021.174136
Received 18 December 2020; Received in revised form 20 April 2021; Accepted 26 April 2021
Available online 30 April 2021

PD drugs currently in use such as levodopa, carbidopa and safinamide cause serious side effects. For the sake of finding safer and effective drugs for curing PD, we selected some indigenous herbs and their active components by inquiring folk pharmacists. Afterword, we chose Acteoside (ACT; Fig. 1A) as a potential drug candidate for PD treatment by reviewing the domestic and foreign literature. Up to date, ACT has been found in more than 200 plant species, e.g., *Cistanches Herba* and *Radix Rehmanniae* (An et al., 2019; Li et al., 2020). ACT has variety of biological activities (Li et al., 2020), e.g., neuroprotective activities (Li et al., 2018; Xia et al., 2018; Kodani et al., 2019). Weather ACT could be

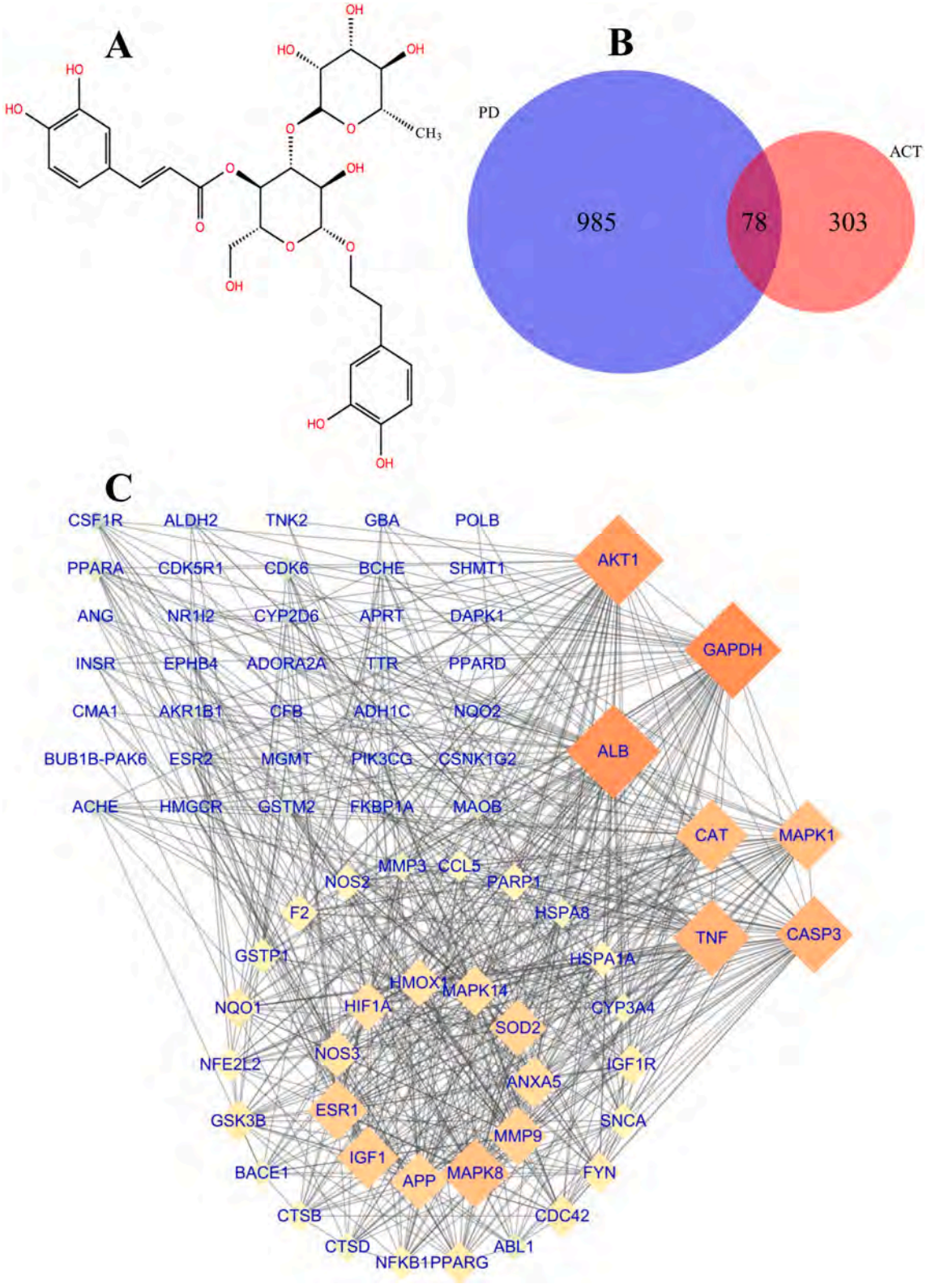

Fig. 1. Venn diagram and network graph. (A) Chemical structure of ACT downloaded from DrugBank database (DB12996, CAS: 61276-17-3); (B) Venn diagram of overlapped targets between ACT potential targets and PD targets; (C) The node-size mapping of the 78 shared targets between ACT potential targets and PD targets.

an effective agent for PD treatment and its underlying molecular mechanisms are largely unknown; especially its relationship with autophagy has not been reported yet.

In the present study, in order to fully explain the interactive protein targets and the related molecular mechanisms of action, we identified drug targets of ACT by analyzing four types of public databases, and the PD-related targets by analyzing public database of DisGeNET. The shared putative targets between ACT and PD were identified for further investigation based on protein-protein interaction, gene ontology (GO), and Kyoto encyclopedia of genes and genomes (KEGG) pathway analysis. Our experimental results proved that in the range of none toxic concentrations, ACT demonstrated as a specific enhancer of autophagy-lysosome pathway, and thereby exerted beneficial effects on multiple pathological processes including cell injury, SNCA aggregation, oxidative stress, and mitochondrial dysfunction in PD cell models; while in ROT –induced PD *D. melanogaster* model, ACT ameliorated movement dysfunction, increased healthy lifespan, and improved neuronal pathologic changes. Electro microscopic imaging results further verified that ACT treatment induced autophagy, thereby prevented cell damage induced by ROT in PC-12 cells. This study for the first time identified that ACT could be a promising candidate drug for the treatment of PD.

2. Materials and methods

2.1. Computational collection of intracellular targets associated with ACT and PD

The structure and Canonical SMILES information of the ACT were found in PubChem (https://pubchem.ncbi.nlm.nih.gov/). Afterward, four public databases including PharmMapper (Liu et al., 2010), ChemMapper (Gong et al., 2013), SwissTargetPrediction (Daina et al., 2019), and ChEMBL (Gaulton et al., 2017) were employed to identify ACT-related targets depending on chemical similarities, pharmacophore models, and published data from medicinal chemistry literature (Liu et al., 2010; Gong et al., 2013; Gaulton et al., 2017; Daina et al., 2019). *Homo sapiens* data were selected, added to all targets identified by using the above four databases for further investigation. The standard gene names and related information of target proteins were obtained from UniProtKB (https://www.uniprot.org/) database by limiting the species with "*Homo sapiens*" (Consortium, 2017). The acknowledged PD-related targets were collected from DisGeNET Database (http://www.disgenet.org/), a database of gene-disease associations, containing publicly available collections of genes and variants associated to human diseases (Piñero et al. 2017, 2020). The standard gene names and related information were validated and obtained from UniprotKB database as well. The ACT-related and PD-related crossover target genes were filtered with R 4.0.2 software using the Venn diagram package.

2.2. Network construction and bioinformatics annotation

We applied STRING 11.0 database (http://string-db.org/cgi/input.pl) and Cytoscape 3.6.1 software to construct a node-size network for putative targets of ACT for the treatment of PD based on their interaction data. All parameters including protein-protein correlation degree, closeness, betweenness, and centralities were analyzed by plugin in Cytoscape 3.6.1 software. The database for annotation, visualization, and integrated discovery (DAVID) Bioinformatics Resource 6.8 (https://david.ncifcrf.gov/), Cluster Profiler (Yu et al., 2012), and ggplot2 (Ito and Murphy, 2013) packages in R 4.0.2 software were used to annotate *P* values and visualize GO and KEGG pathway enrichment.

2.3. Cell culture and stable cell lines

Green fluorescent protein (GFP) - microtubule - associated protein light chain 3 (LC3) (GFP-LC3) stably expressing normal rat kidney (NRK) cells and translocase of the outer membrane 20 (TOM20) – GFP (TOM20-GFP) plasmid were generous gifts from Professor Yu Li (Tsinghua University, CN). A GFP NH_2-terminal-link-SNCA and SNCA-GFP COOH-terminal (GN-link-SNCA and SNCA-GC) stably expressing human embryonic kidney 293 (HEK293) cell line was a kind gift from Professor Jie Qiong Tan (Central South University, CN). Human neuroblastoma cells SH-SY5Y and rat pheochromoytoma cells PC-12 were obtained from cell repository of Chinese Academy of Sciences. NRK, HEK293 and SH-SY5Y cell lines were cultured in Dulbecco's Modified Eagle's Medium (DMEM, Hyclone) containing 10% Fatal Bovine Serum (FBS, Biological Industries), and 1% penicillin-streptomycin solution (10,000 units/ml of penicillin and 10,000 g/ml of streptomycin, Biological Industries). PC-12 cells were grown in DMEM, supplemented with 10% FBS, 5% horse serum (Invitrogen, #16050122), and 1% penicillin-streptomycin solution. The TOM20-GFP stably expressing PC-12 cell line was established as previously described with minor revision (Jiang et al., 2014). Briefly, cells were transfected with TOM20-GFP plasmids using 4D-NucleofectorTM System (Lonza, Germany) according to the manufacturer's instructions. PC-12 cells constitutively expressing TOM20-GFP were selected using 800 μg/ml Geneticin (G418, Invitrogen, #10131027) and maintained in 200 μg/ml G418.

2.4. Cell morphology and cell viability assay

PC-12 cells were seeded in 96-well plates at a density of 10,000 cells/well. On the next day, cells were treated with various concentrations (25, 50, 100, 200, 400 μM) of ACT (HPLC tested purity $\geq$ 99.9%, Shanghai Yuan Ye Bio-Technology, #Y03F9H54484) and various concentrations (0.1, 0.2, 0.4, 0.8, 1.6 μM) of ROT (Sigma Aldrich), and various concentrations of ACT with various concentrations of ROT for additional 24 h, morphological changes of cells were observed by using inverted microscope (Leica CTR 6000, DMI 6000B). Cells were seeded and cultured with the same way in 96-well plates, and treated with 50 μM of ACT and 0.2 μM of ROT, and ACT with ROT for 24, 48, and 72 h, respectively. At the final time point, 0.5 mg/ml 3-[4,5-dimethylthiazol-2-yl]-2,5 diphenyl tetrazolium bromide (MTT, Sigma-Aldrich) was added to the cells and incubated for additional 4 h, and added dimethyl sulfoxide (DMSO, Sigma-Aldrich) to resolve it at room temperature. Light absorption was acquired at 490 nm or 570 nm using a micro plate reader (Thermo Scientific Multiskan FC).

2.5. Crystal violet staining

For crystal violet staining, we modified a method described previously (Jiang et al., 2016). Briefly, 5000 cells/well were seeded in 6-well plates, treated after 10–24 h. On day 4 post-treatment, cells were washed three times with phosphate-buffered saline (PBS, Biological Industries), stained with 0.05% crystal violet in double distilled H_2O for 10–20 min at room temperature, followed by three washes with PBS. Afterward, the plates were air-dried and photographed.

2.6. D. melanogaster stocks and drug feeding

We used wild type *D.melanogaster* from Xinjiang University. Flies were reared on standard cornmeal-molasses medium containing sucrose (10%), yeast extract (2%), agar (1.5%) and corn powder (3.3%) at 23 ± 1 °C. For the treatment of third instar larvae (L3 larvae), ACT and ROT were initially dissolved in DMSO then diluted in liquid medium with 10% sucrose and 1.5% yeast extract to desired concentrations. For starvation group, the liquid medium prepared with 10% sucrose in distilled water. L3 larvae were collected as described elsewhere (Nichols et al., 2012) with minor revision, transferred to corresponding groups, and incubated for indicated time points. For the treatment of adult flies, 2–8 days old adult male flies were transferred for 7 days to flasks containing cotton soaked with a 10% sucrose (BioShop) solution with either DMSO (as control) or 500 μM ROT, or 500 μM ACT, and 10% sucrose with dissolution of same concentration of ROT and ACT (treatmental

flies) as described elsewhere (Doktór et al., 2019) with minor changes.

2.7. Larval crawling assay

For larval crawling assay, we modified a method described previously (Nichols et al., 2012). Briefly, we used 2% agarose in distilled water to make harden transparent medium in 15-cm Petri-dish, and put this dish over a graph paper with 0.2 cm^2 grid, and transported individual L3 larvae to that Petri-dish put over graph paper, and finally measured the trajectory crossed in 1 min.

2.8. LysoTracker staining and quantitative analysis of autophagic structures

L3 larvae were dissected under stereoscope (ECOLINE, ES-39BF) in PBS. The fat bodies were stained with 100 nM of LysoTracker Red DND-99 (Invitrogen, #L-7528) and 200 nM of Hoechst 33342 (Invitrogen, #45885A) in PBS for 5–10 min at room temperature. Fat body lobes were rinsed once in PBS, mounted in 60% glycerol in PBS to a glass slide, and was immediately visualized by laser confocal microscopy (Nikon, Ti-E C2+ confocal microscope system). Quantitative analysis of lysotracker-positive spots was performed according to previously described protocol with minor revision (Lu et al., 2012).

2.9. Climbing assay to test negative geotaxis

After drug treatment, 9–15 days old (N = 15) male flies were transferred into an empty vial according to a previously published method with minor changes (Gargano et al., 2005). After 16 h recovery, flies were gently tapped to the bottom of their vial; individuals climbed vertically beyond a 5-cm marked line were counted. The experiment was carried out in dim white light under constant conditions and was repeated three times.

2.10. Survival test

Lifespan tests were performed at 23 ± 1 °C as described elsewhere (Oxenkrug et al., 2011) with minor changes. After drug treatment, 9–15 days old (N = 30) male flies were collected and then regularly transferred to fresh medium every 3–4 days. The number of dead flies was observed and recorded in every 12 h. The test was carried out between August and December.

2.11. Transmission electron microscopy

2.11.1. D. melanogaster whole brain imaging

Drug treatments were the same as previously described procedure "2.6". After 16 h recovery, the heads of flies were disconnected under stereoscope, and were fixed in cacodyl-buffered paraformaldehyde (2.5%) and glutaraldehyde (2.5%) primary fixative for 2 h, then were post-fixed for 1 h in OsO4 (1%) in veronal acetate buffer. Subsequently, the heads were dehydrated in an alcohol series followed by propylene oxide, then embedded in Poly/Bed 812 resin (Polysciences). Ultrathin sections were cut and contrasted with uranyl acetate and lead citrate. Images of tetrad synapses in the lamina were taken using a JSM1230-TEM (transmission electron microscopy) operating at 80 kV, and projection images were recorded on a MORADAG3 CCD camera (EMSIS, Germany).

2.11.2. PC-12 cell imaging

The cells were cultured in 10-cm petri-dishes. After drug treatment, cells were washed three times with PBS, trypsinized to collect cells, fixed in glutaraldehyde (2.5%) primary fixative for 1–2 h, and rinsed 3 times with PBS (PH 7.2–7.4). Cells were post-fixed for 1 h in OsO4 (1%) in veronal acetate buffer, then rinsed 3 times. Subsequently, the cells were dehydrated in an alcohol series followed by propylene oxide, and then infiltrated, embedded, polymerized, sectioned according to a previous publication with minor modifications (Jiang et al., 2016). We examined 90 nm thin sections using a JSM1230-TEM operating at 80 kV, and projection images were recorded on a MORADAG3 CCD camera.

2.12. GFP-LC3 puncta imaging and counting

After treatment for 24 h, GFP-LC3 stably expressing NRK cell images was acquired using laser confocal microscope. GFP Puncta numbers were counted in cells as described previously with minor revision (Lu et al., 2012). Briefly, the GFP-LC3 puncta in each cell were manually counted, and at least 40 cells were randomly selected for counting in each group. The data presented were from one representative experiment of three independent experiments.

2.13. Mitochondrial isolation and purification

Mitochondria were isolated from SH-SY5Y cells using a Mitochondria Isolation Kit (Solarbio, #SM0020) according to the manufacturer's protocol. Cells were trypsinized and washed twice in PBS. Approximately 1.5 × 10^7 cells were collected and added 1 ml of lysis buffer supplemented with protease inhibitor Cocktail (Sigma-Aldrich, #P8340). The tube was vortexed and incubated on ice for exactly 2 min. Cell lysate was transferred to Dounce Tissue Grinder (pre-chill before use) and homogenized with 50–60 strokes on ice. Cell lysate was returned to the original tube and centrifuged at 1000×*g* for 10 min at 4 °C; supernatants were transferred to a new tube. Then, supernatants were centrifuged at 12,000×*g* for 15 min at 4 °C; supernatants (cytosol fraction) were again transferred to a new tube. The pellet contains the isolated mitochondria, was resuspend with a RIPA lysis buffer (Solarbio, #R0020) supplemented with Protease Inhibitor Cocktails (Thermo Scientific™, #78438). Protein concentration was determined using a BCA Protein Assay Kit (Beyotime Institute of Biotechnology, CN).

2.14. Western blotting analysis

Western blotting (WB) was performed as described elsewhere (Rusmini et al., 2019) with minor revisions. 10–15 μg of protein samples and prestained protein ladders (Thermo Scientific, #26619 and #26625) were loaded onto polyacrylamide gel for electrophoresis, and subsequently transferred to a nitrocellulose (NC) membrane. The membrane was blocked with 5% nonfat dried milk dissolved in PBS with 0.3% Tween-20 (PBST) for 45 min. After washing in PBST, NC membrane was incubated with primary antibody for 1 h at room temperature or overnight at 4 °C, washed in PBST, followed by incubation with corresponding horseradish peroxidase coupled secondary antibodies for 1 h at room temperature. After washing in PBST, the membrane was treated with Immobilon™ Western chemiluminescent substrate (MILLIPORE, #WBKLS0500), immediately visualized using a chemiluminescence system (ProteinSimple, USA) or exposed to X-ray film in darkroom. The antibodies used are as follows: anti-LC3A/B (#L7543, 1:10,000), anti--β-actin (#A2066, 1:10,000), anti-Cleaved-Caspase-3 (#C8487, 1:1000), and anti-SQSTM1 (#P0067, 1:1000) were purchased from Sigma-Aldrich. Anti-phospho-p70S6K (Thr389, #9234, 1:1000) and anti-phospho-AMPK (Thr172, #2535, 1:1000), anti-a-synuclein (#2628, 1:1000), and anti-COX IV (#4844, 1:1000) were purchased from Cell Signaling Technology. Anti-mTOR (#ab134903, 1:5000), anti-phospho-mTOR (S2448, #ab1109268, 1:5000), anti-Pro-Caspase-3 (#ab13847, 1:1000) and anti-Bax (#ab32503, 1:1000) were purchased from Abcam. Anti-GAPDH (#AF7021, 1:1000) was purchased from Affinity. The secondary antibodies peroxidase conjugated goat anti-rabbit IgG-HRP (#4010-05) and goat anti-mouse (#1070-05) were purchased from Southern Biotech.

2.15. Detection of SNCA expression

After treatment for 24 h, the GN-link-SNCA and SNCA-GC stably expressing HEK293 cells were reacted with 100 nM LysoTracker Red and 200 nM Hoechst 33342 for 15 min at 37 °C. After washed twice in cold PBS, the live cells were visualized under a laser confocal microscope. The GFP-SNCA fluorescence intensity relatively represents α-synuclein expression level.

2.16. Annexin-V/7AAD staining

After treatment for 24 h, PC-12 cells in each group were trypsinized and washed twice. Subsequently, the cells were incubated with PE Annexin V Apoptosis Detection Kit I (BD Pharmingen™, #559763) in the presence of ~400 μl binding buffer for 20 min at room temperature in the dark. About 50,000 cells were acquired and analyzed by BD LSR II flow cytometer.

2.17. Intracellular ROS detection and mitochondrial morphology analysis

After treatment for 24 h, the intracellular ROS generation of PC-12 cells was detected using 2′, 7' -dichlorofuorescein-diacetate (H_2DCF-DA; EMD Millipore, #287810) by minor modification of a previously described method (Lu et al., 2016). Briefly, after drugs treatment, cells were incubated with the probe H_2DCF-DA working solution (25 μM) for 20 min at 37 °C. Thereafter, cells were washed with cold PBS three times to remove the unbound dye. A laser confocal microscope was used to evaluate the fluorescence of ROS production with the Image J software.

To observe the mitochondrial morphology, following drug treatment for 24 h, the PC-12 cells were reacted with 100 nM MitoTracker Red CMXRos probe (Invitrogen, #M22425) for 15 min at 37 °C. After being washed twice in cold PBS, the live cells were visualized under a laser scanning microscope. Fragmented and damaged mitochondria were shortened, punctate, and sometimes gather around the nucleus, whereas healthy or fusioned mitochondria showed a rod-like or long thread-like tubular structure.

2.18. Measurement of mitochondrial membrane potential (Δψm)

Δψm is a widely used marker for mitochondria damage. To measure the Δψm, JC-1 kit (Beyotime Institute of Biotechnology, #C2006) was used according to the manufacturer's instructions. Briefly, after the drug treatment for 24 h, cells were washed twice with PBS, and incubated with JC-1 solution for 20 min at 37 °C. Afterward, the fluorescence emissions were acquired by laser confocal microscope, the ratio of red-to-green fluorescence intensities were calculated using Image J software to reflect Δψm. When mitochondria were healthy, JC-1 forms J-aggregates at high Δψm and emits redder fluorescence. Meanwhile, when mitochondria were damaged, JC-1 remains in monomer forms at low Δψm and emits greener fluorescence.

2.19. Confocal microscopy analysis for mitophagy detection

After treatment for 24 h, the TOM20-GFP stably expressing PC-12 cells were reacted with 100 nM LysoTracker Red for 15 min at 37 °C. Washed twice in cold PBS, the live cells were visualized under a laser confocal microscope. The degree of colocalization (yellow fluorescence intensity) of TOM20-GFP with lysosome represents mitophagy (mitochondrial autophagy) occurrence level.

3. Results

3.1. Target identification, shared targets between ACT and PD

381 potential targets of ACT were predicted by using four different target fishing approaches as described in method section, and 1063 PD-related potential targets were obtained by DisGeNET Database, among them 78 shared targets between ACT and PD (Fig. 1B) were selected for further investigation. Afterward, the node-size mapping of these shared targets was made. As shown in Fig. 1C, 18 proteins were identified as the potential key targets of ACT against PD including Glyceraldehyde-3-phosphate dehydrogenase (GAPDH), Serine/threonine kinase 1 (AKT1), Albumin (ALB), Caspase-3 (CASP3), and mitogen activated protein-kinase (MAPK) are the key targets with the largest node size according to "Degree" in the node size mapping, the size and color depth of nodes are proportional to the degree of centrality by topology analysis.

3.2. GO and KEGG pathway analysis

To further investigate the 78 shared targets of ACT and PD-related potential targets, we performed the interaction network regulation analysis by using DAVID database and R 4.0.2 packages of Cluster Profiler and ggplot2. As shown in Fig. 2, we have tabulated top 15 GO mapping of Molecular Function (Fig. 2A), Cellular Component (Fig. 2B), and Biological Process (Fig. 2C). We have identified top 30 KEGG pathways out of 78 shared targets (Fig. 2D). Interestingly, the KEGG pathway-enrichment analysis showed that most pathways mentioned here are closely related to autophagy and apoptosis.

3.3. ACT protects PC-12 cells from ROT induced toxicity

To further investigate the neuroprotective activities of ACT, we treated PC-12 cells with different concentrations of ACT and ROT for various time points 24, 48, 72, and 96 h. We have found that ACT itself is not cytotoxic to PC-12 cells in the concentration range of 0–200 μM, and showed neuroprotective activities to the cell injuries toxicated by in the concentration range of 0–0.4 μM ROT (data not shown). Treatment of PC-12 cells with 50 μM ACT alleviated cell injury induced by 0.2 μM ROT (Fig. 3A), and the protective effects increased by time (Fig. 3B). ACT treatment increased PC-12 cell survival compared with that in ROT treatment. The colony formation assay further confirmed the protective effects of ACT on ROT-induced neuronal cell injury (Fig. 3C).

3.4. ACT improves motor impairment and lifespan, and ameliorates brain pathology in ROT induced PD model of D. melanogaster

The analysis of larval crawling trajectory test elucidated that 500 μM ACT feeding had no toxicity to L3 larvae of *D. melanogaster*. In 250 μM ROT treatment group, the distance travelled was significantly shortened, indicating obvious locomotor impairment (Fig. 4A and B). The analysis of *D. melanogaster* climbing test revealed that ACT treatment increased the climbing ability of flies treated with ROT compared to the group treated with ROT only (Fig. 4C). Lifespan tests have showed that ACT feeding partially prevented the early death of *D. melanogaster*, but it does not take effect after 80 days of life interval (Fig. 4D). TEM micrographs (Fig. 4E) of brain tissues of *D. melanogaster* showed mitochondria injury and synapse distortion after exposure to ROT. Flies fed with ROT exhibited the altered shape of synaptic vesicles: less visible, with a slightly broken membrane, the vesicles are lighter. The mitochondria also become smaller, less visible, almost broken. In flies fed with ACT and ROT, the synaptic vesicles were mostly round, electron dense, and the morphology of mitochondria returned to normal. ACT treatment restored correct morphology of mitochondria and synaptic vesicles.

3.5. ACT induces autophagy in D. melanogaster

Fat bodies of L3 larvae or adult *D. melanogaster* are sensitive to autophagic stimuli and can be visualized by using lysotropic dye (Lu et al., 2012). In our study, L3 larvae of *D. melanogaster* were fed with 100 μM and 500 μM of ACT for 6 h; another group of L3 larvae starved for 3 h to induce autophagy, fat bodies were then isolated and subjected

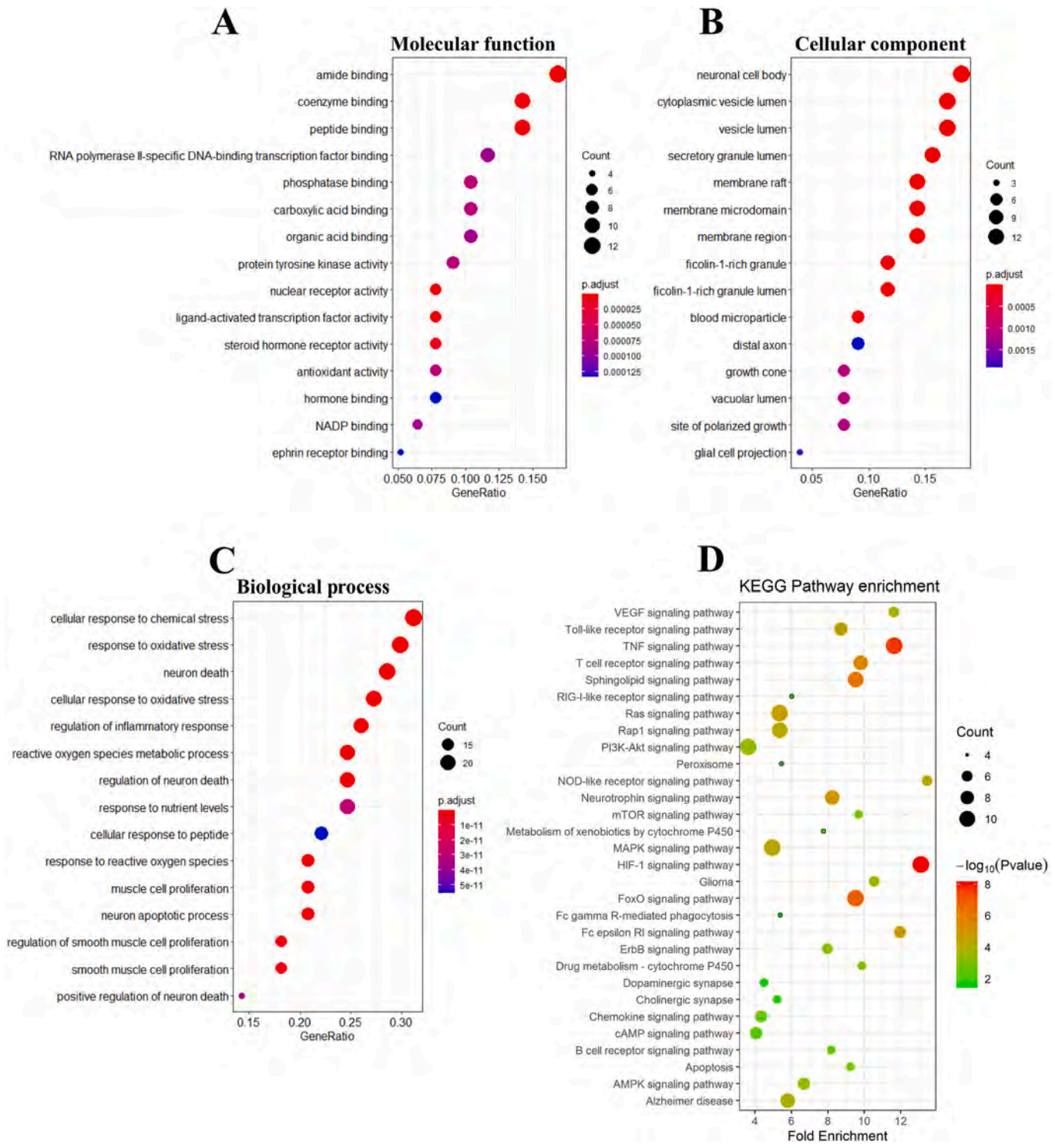

Fig. 2. Functional analysis of therapeutic targets. (A, B, and C) The GO enrichment analysis of the 78 putative targets with dot plot for top 15 molecular function, top 15 cellular component, and top 15 biological process. (D) The top 30 KEGG pathway enrichment analysis of 78 putative targets with dot plot.

to Hoechst 33342 and LysoTracker Red staining. We found that ACT feeding induced the formation of LysoTracker Red puncta in the L3 larvae fat bodies in a similar pattern to starvation (Fig. 5). These data suggested that ACT can induce autophagy in our *in vivo* model, the fat bodies of *D. melanogaster* (L3 larvae).

3.6. ACT induces autophagy by enhancing AMPK phosphorylation in vitro

To identify key signaling passway(s) involved in autophagy induction, we used GFP-LC3 constitutively expressing NRK cell line as a model. According to network pharmacology analysis and literature inquiry, we identified ACT as a potent neuroprotection agent and autophagy inducer which induced massive GFP-LC3 puncta formation in the NRK GFP-LC3 cells (Fig. 6A and B). Moreover, ACT treatment promoted

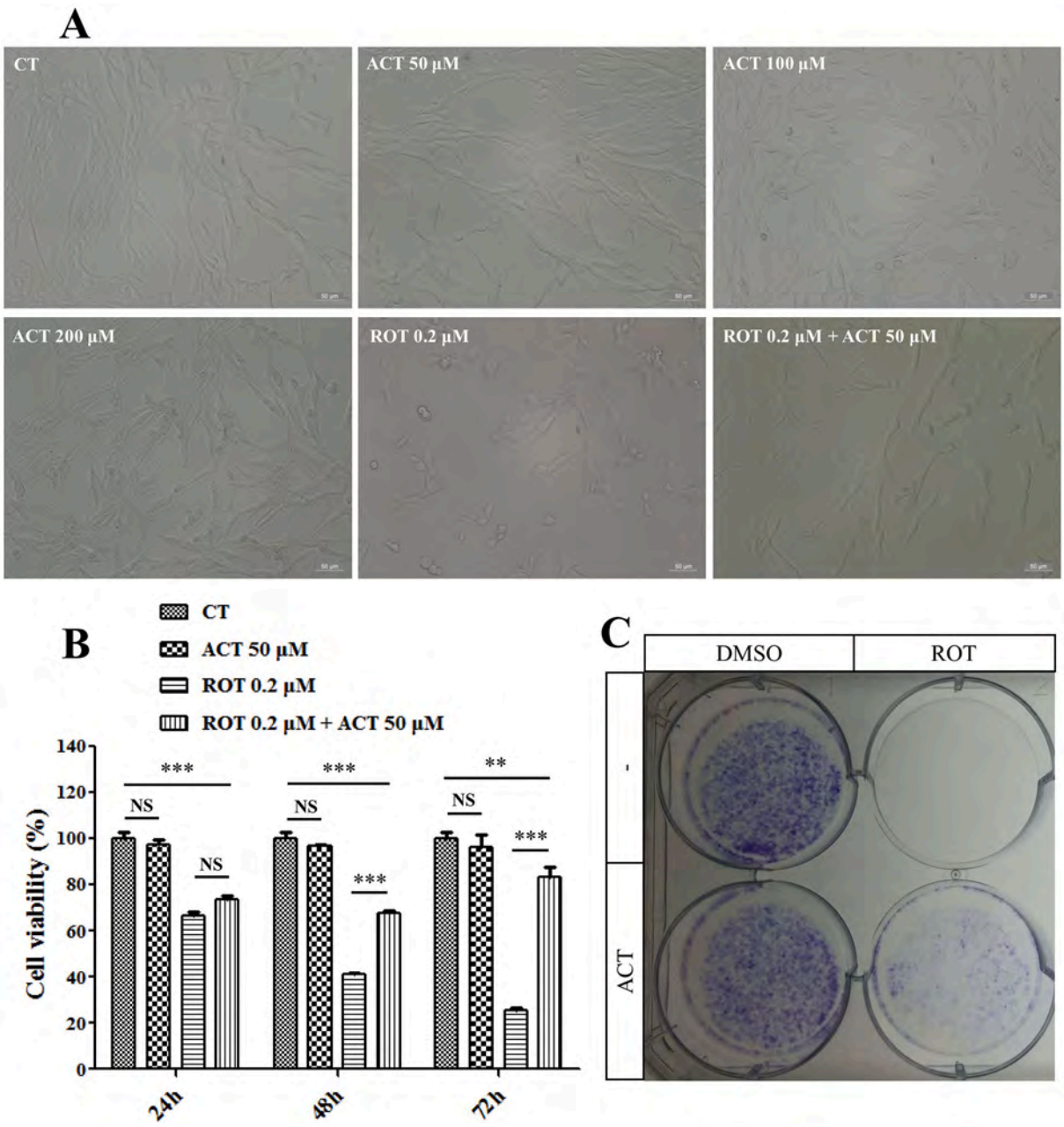

Fig. 3. ACT attenuated PC-12 cells injury induced by ROT. (A) Cytotoxicity was observed via cellular morphological changes, ACT has no toxic effects on PC-12 cells in the range of 0–200 μM, and 50 μM ACT partially protected PC-12 cells from 0.2 μM ROT -induced injury, representative images are shown. (B) Cytotoxicity was measured by MTT conversion. ACT demonstrated a damage repair effect on PC-12 cells in a time-dependent manner. Data were presented as mean ± S.E.M. of three independent experiments. (*$P < 0.05$, **$P < 0.01$, ***$P < 0.001$, one-way ANOVA for multiple comparison and Newman-Keuls test as post hoc test). (C) Viable cells were visualized by crystal violet staining; PC-12 cells were treated as indicated in a 6-well plate. After 96 h, colony formation was observed by staining with crystal violet. As expected, the toxic effects of ROT are prevented by incubation of the cells with ACT.

the conversion of LC3-I to LC3-II in PC-12 cells in some extent, though the difference was not statistically significant (Fig. 6C and D). In order to understand the autophagic mechanism of ACT action, we first examined the mammalian target of rapamycin (mTOR) and 5′ adenosine monophosphate activated protein kinase (AMPK) pathways. We found that ACT treatment enhanced AMPK phosphorylation, but did not affect the mTOR, phosphorylated mTOR and phosphorylated p70 ribosomal protein S6 kinase (p-p70S6K) (Fig. 7), indicating that ACT induces autophagy in neuronal cells in an AMPK-dependent but mTOR-independent manner. Interestingly, besides AMPK signaling pathway, there are other pathways including MAPK, Hypoxia inducible factor 1 (HIF1), Phosphoinositide-3-kinase (PI3K) -Akt, and Forkhead box O (FoxO) pathways were also identified to be involved in the activation of autophagy by network pharmacology approach (Fig. 2D).

3.7. ACT greatly reduces the accumulation of constitutively over-expressed SNCA species in HEK293 cells through inducing autophagy

Safe and effective inducers of autophagy are believed to be the most beneficial candidate drugs for treatment of PD by promoting the clearance of pathogenic proteins such as SNCA. In our study, we examined ACT -induced clearance of SNCA in GN-link-SNCA and SNCA-GC stably expressing HEK293 cells. As shown in Fig. 8, ACT promoted the degradation of SNCA oligomers as illustrated by decreased fluorescence

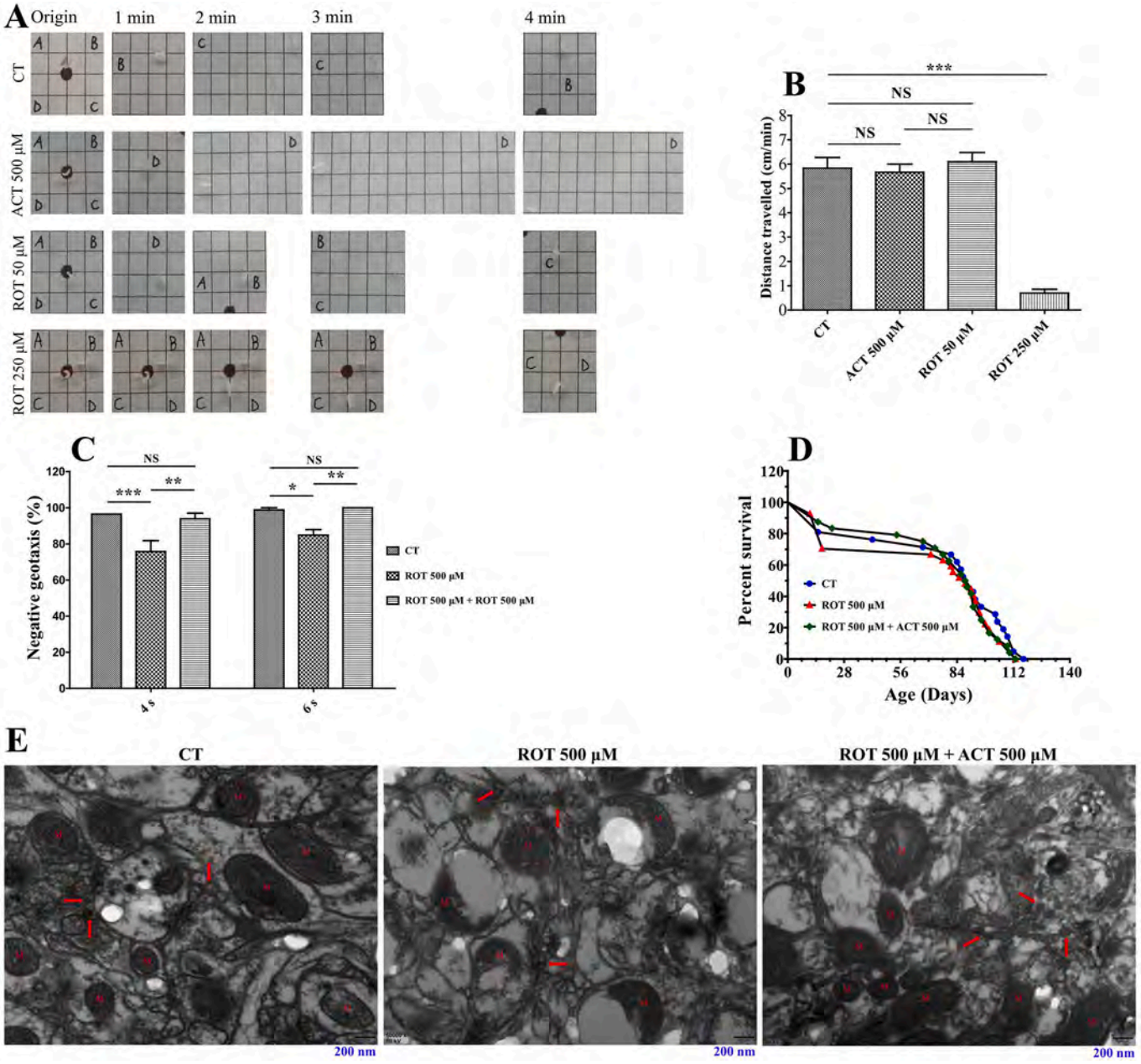

Fig. 4. ACT attenuated *D. melanogaster*'s injury induced by ROT. ACT partly restored *D. melanogaster*'s motor activity. (A) A representative row data from a larval crawling assay using L3 larvae after 6 h of ROT exposure and ACT treatment. (B) Larval crawling assay for L3 larvae. Data were presented as mean ± S.E.M. of three independent experiments. (***$P < 0.001$, one-way ANOVA for multiple comparison and Newman-Keuls test as post hoc test). (C) *D. melanogaster* climbing assay. ROT exposure significantly affected the climbing ability of *D. melanogaster*, thus ACT co-treatment restored this form of activity in ROT-treated subjects. Data were presented as mean ± S.E.M. of three independent experiments. (**$P < 0.01$, two-way ANOVA for multiple comparison and Bonferroni post test as post hoc test). (D) Lifespan test for *D. melanogaster*. ROT exposure affected the early lifespan of *D. melanogaster*, and ACT treatment slightly ameliorated ROT-induced impaired lifespan on *D. melanogaster*. (E) TEM micrographs of brain tissues of *D. melanogaster*. ACT treatment restored the normal morphology of these synaptic vesicles and mitochondria in these flies injured by ROT: they are more visible, and the Mitochondria "M" are integrated, better visible, (Red Arrow - synaptic vesicles).

intensity, and proportionately reduced SNCA levels which can be blocked by an autophagy inhibitor 3-Methyladenine (3-MA, #5142-23-4, Sigma-Aldrich). The observed clearance of SNCA by ACT was found to be at least partly dependent on the autophagy-lysosome pathway, because 3-MA proportionately abolished the pro-clearance activity of ACT, while autophagy inducer Rapa decreased fluorescence intensity, but did not effect on SNCA levels (Fig. 8).

3.8. ACT decreases ROT -induced apoptotic rate of PC-12 cells via inducing autophagy

ROT-induced PC-12 cell apoptotic rate was about 15.27%, much greater than that of control cells (5.17%). When ACT was added to ROT treated PC-12 cells for 24 h, the apoptotic rate was decreased to 8.27%, much lower compared with ROT-only treatment group. But the observed ACT effect was blocked by the addition of 3-MA. When 3-MA, ACT, and ROT were simultaneously added to PC-12 cells, the apoptotic rate was 15.57%, similar to the level of ROT treatment group (Fig. 9A and B). The expression levels of apoptosis-related proteins Bcl-2 associated X protein

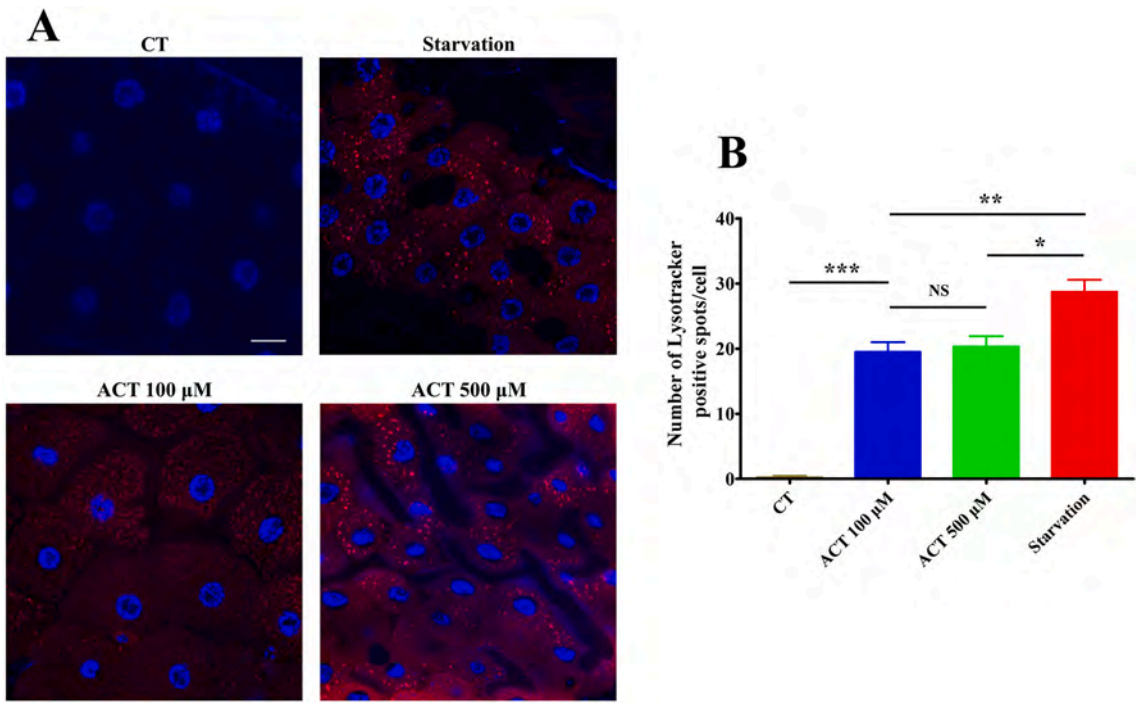

Fig. 5. ACT induced autophagy in fat bodies of *D. melanogaster* (L3 larvae). (A) 96 h after egg laying, the L3 larvae were collected and fed on culture medium containing 500 μM of ACT for 6 h and fat bodies were isolated for LysoTracker staining. Images were captured using a confocal microscope. As a positive control, a group of L3 larvae was starved for 3 h to induce autophagy. (B) Quantification of lysotracker-positive spots in each group as described in panel (A). Data were presented as mean ± S.E.M. of three independent experiments. (*$P < 0.05$, **$P < 0.01$, ***$P < 0.001$, one-way ANOVA for multiple comparison and Newman-Keuls test as post hoc test).

(Bax) and Caspase-3 were in consistance with these results (Fig. 9C and D).

3.9. ACT protects PC-12 cells against ROT -induced mitochondria injury and suppresses ROS generation via inducing autophagy

Mitochondria dysfunction is involved in PD pathology (Sekigawa et al., 2013). Mitochondria complex I inhibitor ROT decreases mitochondrial Δψm, thereby induces mitochondria dysfunction in neuronal cells. In our study, we used MitoTracker Red to investigate the mitochondria pathological changes. Our data showed that mitochondria were impaired in ROT treated group, and the impairment was reversed by the addition of ACT to PC-12 cells treated with ROT, indicating that ACT treatment resulted in rescued mitochondrial morphological integrity, sustained mitochondrial homeostasis. And this protection was abolished by the addition of an autophagy inhibitor 3-MA (Fig. 10). To further investigate the protective role of ACT on ROT -induced mitochondria impairment, we used JC-1 probe to measure mitochondria Δψm in various conditions. Our data indicated that ROT caused a significant reduction of mitochondrial Δψm, while the mitochondria injury (decreased mitochondrial Δψm) was substantially prevented by a 24 h co-treatment with ACT, and the prevention was abolished by the addition of 3-MA (Fig. 11). Furthermore, we used H_2DCF-DA probe to measure the level of ROS generation. We found that ROS production was remarkably increased in ROT treatment, the increment effect was reversed by the co-treatment with ACT, finally the reversal effect was abolished by the addition of 3-MA (Fig. 12), indicating that ACT reduced ROT -induced ROS production via inducing autophagy.

3.10. ACT reverses ROT -induced impairment of mitophagy

To investigate the effect of ACT on ROT-induced mitophagy imbalance, we established TOM20-GFP stably expressing PC-12 cell line as a model for mitochondrial function measurement. The data showed that ACT treatment enhanced mitophagy and did not cause cellular damage, while ROT treatment enhanced mitophagy but induced serious cell injury. As expected, co-treatment with ACT prevented ROT-induced cell injury via promoting mitophagy proportionately in PC-12 cells (Fig. 13A). Our results indicated that ACT abolished ROT-related mitochondria impairment in PC-12 cells and reversed cellular injury via enhancing mitophagy. To confirm the mitophagic changes, cytosolic and mitochondria proteins from SH-SY5Y cells in various treatment conditions were extracted and analyzed by WB. WB analysis elucidated that the ACT treatment caused the translocation of autophagy-related proteins LC3 II and Sequestosome 1 (p62/SQSTM1) to mitochondria, while ROT treatment almost did not induce translocation of LC3 II and SQSTM1 to mitochondria. Co-treatment of SH-SY5Y cells with ACT and ROT also caused the translocation of autophagic proteins to mitochondria (Fig. 13B, C, D). To further investigate the effects of ACT on ROT -induced cell injury and mitophagy imbalance, we used TEM microscopy to observe sub-cellular changes of PC-12 cells under various treatment conditions. The results showed that ROT caused severe cell injuries and increased the number of mitochondria, but most of them became smaller and abnormal. Co-treatment with ACT for 24 h substantially prevented from the cell injury induced by ROT, since the number and size of mitochondria were observed to be nearly normal. And we also observed autolysosome and the initiation of mitophagic structures in the co-treated cells (Fig. 14).

4. Discussion

We identified that 78 putative targets are closely related to ACT treatment of PD by using drug and disease target fishing analysis; among these targets we selected 18 hub targets for further investigation (Fig. 1B and C). These putative targets have been identified previously in neurodegenerative diseases including PD. For example, GAPDH protects from mitochondria dysfunction and cell injury through enhancing mitophagy in the pathology of Huntington's disease (Hwang et al.,

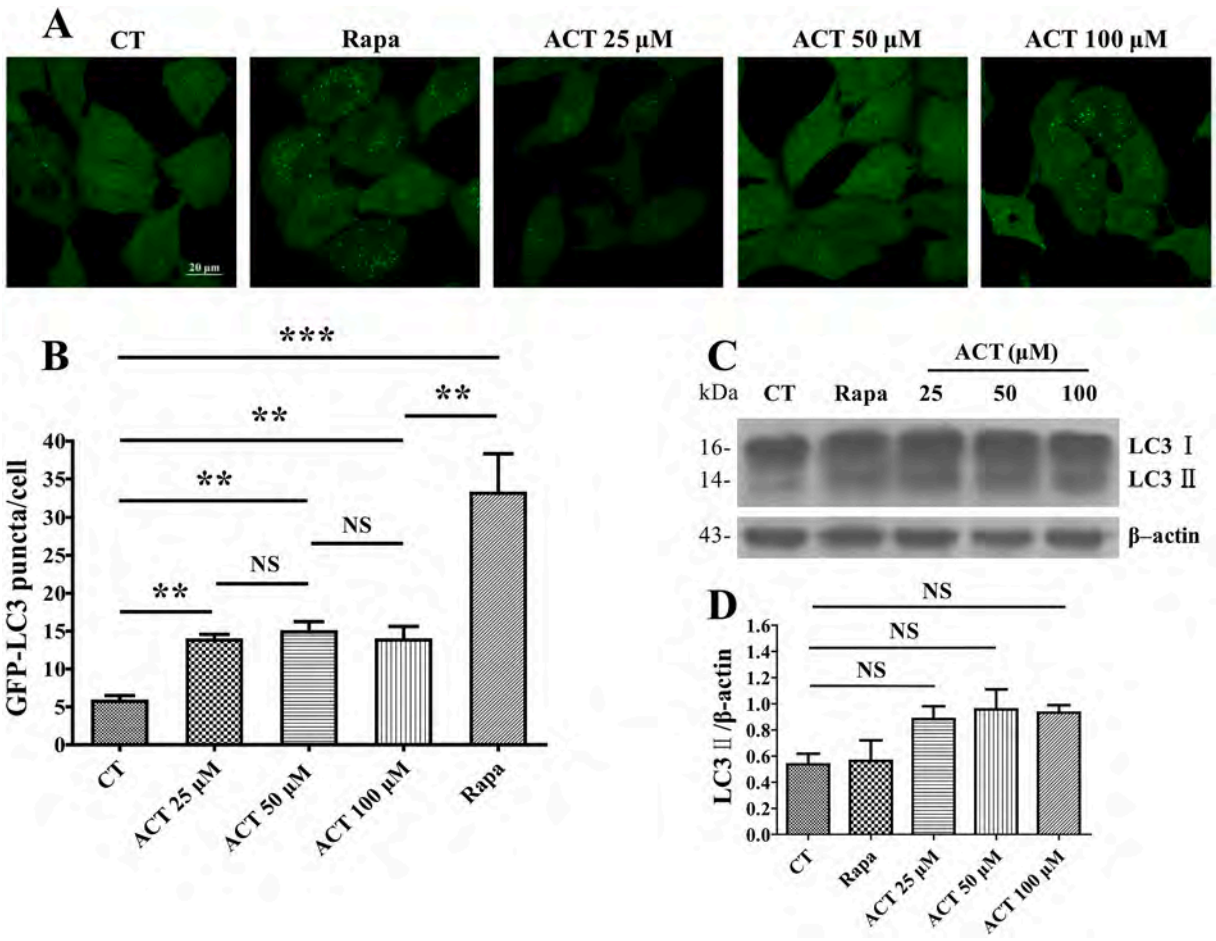

Fig. 6. ACT increased autophagic markers in different cells. (A) GFP-LC3 stably expressing NRK cells were treated with different concentrations of ACT and 100 nM Rapamycin (Rapa, LC Laboratories, R5000) for 24 h. The formation of GFP-LC3 puncta was observed under a laser confocal microscope. (B) Enumeration of GFP-LC3 puncta numbers in each group was performed under the microscopy. Data were presented as mean ± S.E.M. of four independent experiments. (One-way ANOVA for multiple comparison and Newman-Keuls test as post hoc test). (C, D) PC-12 cells were treated with different concentrations of ACT and 100 nM Rapa for 24 h, and cell lysates were subjected to WB analysis. Data were presented as mean ± S.E.M. of four independent experiments. (One-way ANOVA for multiple comparison and Newman-Keuls test as post hoc test).

2015). It has also been reported that decreasing nuclear translocation of GAPDH in PD may exert a potential therapeutic effect (Sekar and Taghibiglou, 2020). AKT1 is a potent mediator of cell growth and survival, involved in protection from PD through many different signaling pathways (Xiromerisiou et al., 2008). ALB is the most abundant protein in plasma, which has multiple functions, and directly exerts neuroprotective actions in neuronal and glial cells (Prajapati et al., 2011). CASP3 is a primary apoptosis-related cysteine peptidase. It has been reported that ACT binds to CASP3 and exerts neuroprotection in the ROT -induced rat model of PD (Yuan et al., 2016). In our study, ACT decreased the Pro-Caspase-3 and Cleaved-Caspase-3 protein expression levels and exerts anti-apoptosis in the ROT -induced cellular model of PD. Studies identified that MAPK signaling pathway is often disregulated in neurodegenerative diseases including PD (Obergasteiger et al., 2018). In this study, ACT may exerts neuroprotection roles in PD models partly through regulating the expression levels or enzymatic activities of MAPK1, MAPK8, and MAPK14. Catalase (CAT) is a crucial antioxidant enzyme, CAT malfunction or deficiency often related to the pathogenesis of many age-associated degenerative diseases like PD (Nandi et al., 2019). Tumor necrosis factor (TNF) including TNF-α signaling mediates neuro-inflammatory events, and plays an important role in the pathogenesis of PD (Çomoğlu et al., 2013; Probert, 2015). Matrix metallopeptidase 9 (MMP9) was reportedly associated with neuro-inflamation, and involved in the pathogenesis of PD (Rempe et al., 2016). AnnexinA5 (ANXA5) related to the stimulation of extracellular regulated protein kinases (ERK) pathway was identified as a new therapeutic target in the treatment of PD (Dong et al., 2018). Superoxide dismutases (SODs) are playing a pivotal role in the antioxidant response; as SOD2 overexpression was able to rescue the pathological phenotypes in experimental PD models (Biosa et al., 2019). Heme oxygenase-1 (HMOX1) up-regulation followed by a parallel activation of other enzymes is associated to cell adaptation and cytoprotection, but the excessive activation of HMOX1 easily produce a deleterious cytopathic effect in PD pathogenesis (Nitti et al., 2018). HIF1A plays pivotal roles in the development and survival of dopaminergic neurons, and therapeutic activation of HIF1A may exert a neuroprotective effect in the treatment of PD (Kandil et al., 2019). Nitric oxide synthase 3 (NOS3) may have a pivotal role in human neurodegenerative diseases, including PD; modulation of NOS3 function may beneficially attenuate the progression of PD (de la Monte et al., 2007; Kapoor, 2012). Estrogen receptor ESR1 and estrogen modulation have protective effects on PD pathogenesis that is probably associated with the lower incidence rates of PD in women compared with men at all ages (Chung et al., 2011; Villa et al., 2016). Insulin like growth factor 1 (IGF1) and insulin may alleviate PD pathology via triggering the PI3K/Akt/glycogen synthase kinase 3β (GSK3β) signaling pathway (Yang et al., 2018). Amyloid beta precursor protein (APP) is the primary constituent of amyloid plaques found in the brains of Alzheimer's disease (Rice et al., 2019). It has been identified that APP interacts with leucine-rich repeat kinase 2 (LRRK2), which is a PD-related protein, plays pivotal roles associated with diverse cellular

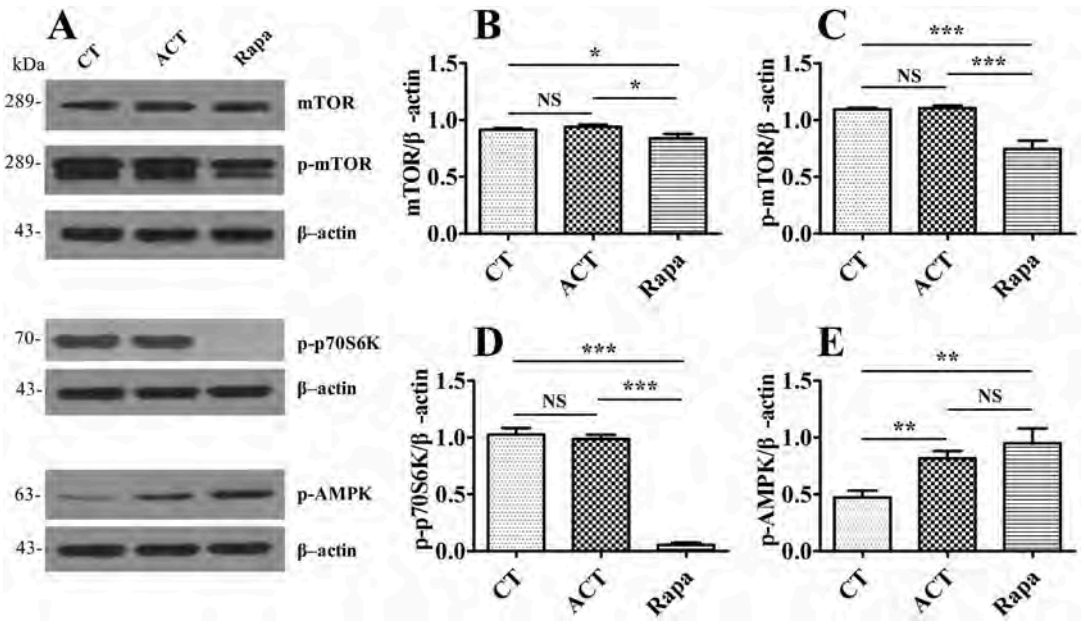

Fig. 7. ACT induced autophagy in PC-12 cells in AMPK -dependent but mTOR -independent manner. PC-12 cells were treated with 50 μM ACT and 100 nM Rapa for 12 h, and cell lysates were subjected to WB analysis. Data were presented as mean ± S.E.M. of three or four independent experiments. (*$P < 0.05$, **$P < 0.01$, ***$P < 0.001$, one-way ANOVA for multiple comparison and Newman-Keuls test as post hoc test).

mechanisms in PD pathogenesis (Lim et al., 2019). To sum up, ACT could be a potential drug candidate for treating PD pathogenesis via modulating above mentioned targets involved in apoptosis and autophagy processes. Further studies may be necessary to confirm the therapeutic potential of ACT on PD.

According to PD pathogenesis and current therapeutic strategies, the following cellular processes modulation therapies are essential for effective treatment. For example, lysosome-autophagy pathway, ubiquitin-proteasome pathway, Calcium signaling, inflammation, apoptosis/necrosis, genomic instability, metabolism, ROS generation, and mitochondrial turnover are all or partially involved in PD pathogenesis. To sum up, PD patients have specific epidemiological factors according to their living environment, genetic susceptibility, age, and sex. Optimal personalized therapies would allow adopting the best supportive measures, e.g., modulating lysosomal-autophagy therapy for patients with a dysfunctional autophagic response, and enhancing proteasome activity therapy for patients with aggregation-prone protein accumulation. The GO and KEGG pathway analysis indicated that ACT possesses pleiotropic effects on modulating multiple signaling pathways to treating PD (Fig. 2).

After further analysis of potential targets, GO and relevant signaling pathways, we concluded that ACT possesses strong pharmacological activities against PD. Our data guide us to further investigate triggering autophagy process (including mitophagy), preventing apoptosis, clearing aggregated proteins (including SNCA), and ameliorating mitochondrial functions in our experimental models. Hence, we have experimentally validated the involvement of SNCA, apoptosis (CASP3), and AMPK phosphorylation in the therapeutic activity of ACT against PD, and these results are highly consistent with network pharmacology analysis (Figs. 1C, 2 and 7, 8, 9).

D. melanogaster has a short life cycle and convenient access, which made this organism an ideal model for studying a wide range of biological processes including locomotive ability, aging, autophagy, genetics and pathogenesis (Gargano et al., 2005; Neufeld, 2008; Oxenkrug et al., 2011). In our study, we have elucidated that ACT not only protects from cytotoxicity induced by ROT in PC-12 cells (Figs. 3 and 14), but also enhances locomotive ability, slightly increases lifespan, ameliorates from neuronal cell injury, and synaptic vesicle impairments caused by ROT in *D. melanogaster* (Fig. 4).

Autophagy, a normal biological process and as well as a cytoprotective mechanism, is particularly crucial in the aging brain and during neurodegeneration (Rubinsztein et al., 2007). Our study revealed that ACT induces autophagy in *D. melanogaster* L3 larvae fat body (Fig. 5) as well as in NRK and PC-12 cells (Fig. 6), indicating that ACT is an inducer of autophagy in neuronal cells. We further confirmed that ACT induces autophagy dependent on the function of AMPK phosphorylation, but independent on the mTOR pathway (Fig. 7). Promoting autophagy has been suggested as a promising therapeutic strategy against neurodegenerative diseases by means of clearing anomaly aggregated proteins, e.g. a-synuclein in PD, tau and β-amyloid in Alzheimer's disease, and Huntington protein in Huntington's disease (Fecto et al., 2014). Our study identified a potent neuroprotection agent ACT, which is able to promote the clearance of aggregate forms of SNCA in GN-link-SNCA and SNCA-GC stably expressing HEK293 cells through inducing autophagy (Fig. 8). Furthermore, ACT treatment reduces the rate of apoptotic cell death (Fig. 9), modulates the imbalanced mitochondrial homeostasis (Fig. 10), increases mitochondrial Δψm (Fig. 11), and inhibites ROS generation (Fig. 12) caused by ROT via inducing autophagy.

PD pathogenesis is usually linked with defective autophagy and damaged sub-cellular organelles in neurons, especially linked with disordered mitochondrial dynamics in neuronal cells (Archer, 2013; Pickles et al., 2018; Hou et al., 2020). Mitochondrial quality and integrity in cells are maintained by the processes of mitophagy and mitochondrial biogenesis (Scheibye-Knudsen et al., 2015; Fang et al., 2019). Mitophagy, the lysosomal-autophagic process of selectively removing damaged mitochondria, was compromised in PD patients and experimental PD models, and was found to be reversely correlated with accelerated neurodegeneration (Liu et al., 2019). Impaired removal of defective mitochondria is a pivotal event in PD pathogenesis, while mitophagy enhancement is a potential therapeutic intervention. Our study revealed that ACT induces mitophagy in PC-12 and SH-SY5Y cells, protects from cell injuries caused by ROT (Figs. 13 and 14), indicating that ACT is a safe enhancer of mitophagy.

ACT is a phenylethanoid glycoside, has been found in many medicinal plants which commonly used for the treatment of symptoms relevant to neurodegenerative diseases including PD. ACT, in our study demonstrated robust potential to induce autophagy in both *in vitro* and *in vivo* models (Figs. 5 and 6). Pharmacological activities of autophagy

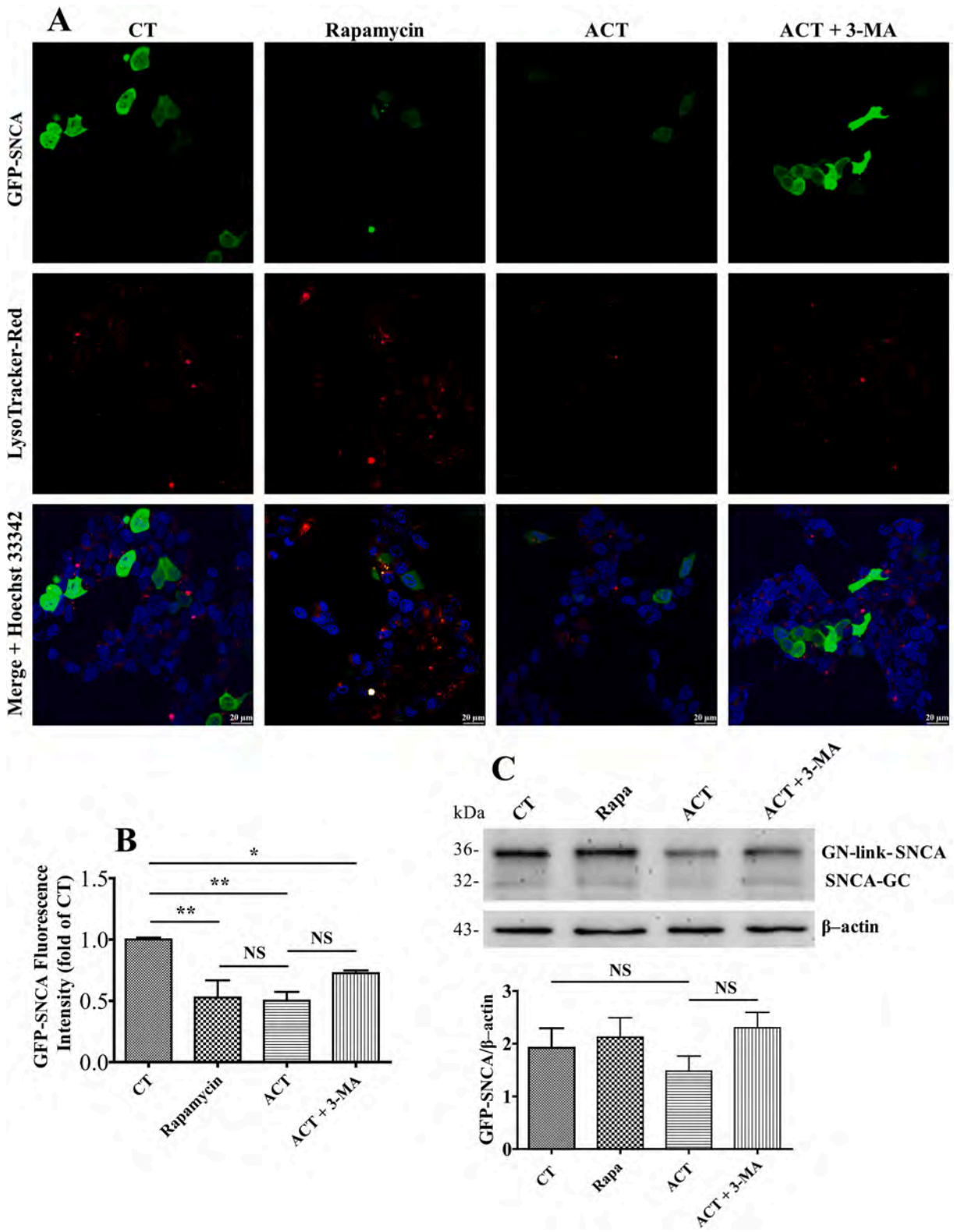

Fig. 8. ACT decreases the accumulation of pathogenic SNCA species in GN-link-SNCA and SNCA-GC stably expressing HEK293 cells. (A) GN-link-SNCA and SNCA-GC stably expressing HEK293 cells were treated with 50 μM ACT, 100 nM Rapa or 5 mM 3-MA as indicated for 24 h. Cells were stained with 200 nM Hoechst 33342 and 100 nM LysoTracker-Red and analyzed under confocal microscope. (B) Quantification of GFP-SNCA fluorescence intensity of cells with aggresomes as described in panel (A), ACT partially decreased the accumulation of SNCA aggresomes, while the observed ACT activity was completely blocked by 3-MA. Data were presented as mean ± S.E.M. of three independent experiments. (*$P < 0.05$, **$P < 0.01$, one-way ANOVA for multiple comparison and Newman-Keuls test as post hoc test). (C) GN-link-SNCA and SNCA-GC stably expressing HEK293 cells were treated with 50 μM ACT, 100 nM Rapa or 5 mM 3-MA as indicated for 24 h. Cell lysates were subjected to WB analysis. Data were presented as mean ± S.E.M. of three independent experiments. (One-way ANOVA for multiple comparison Newman-Keuls test as post hoc test).

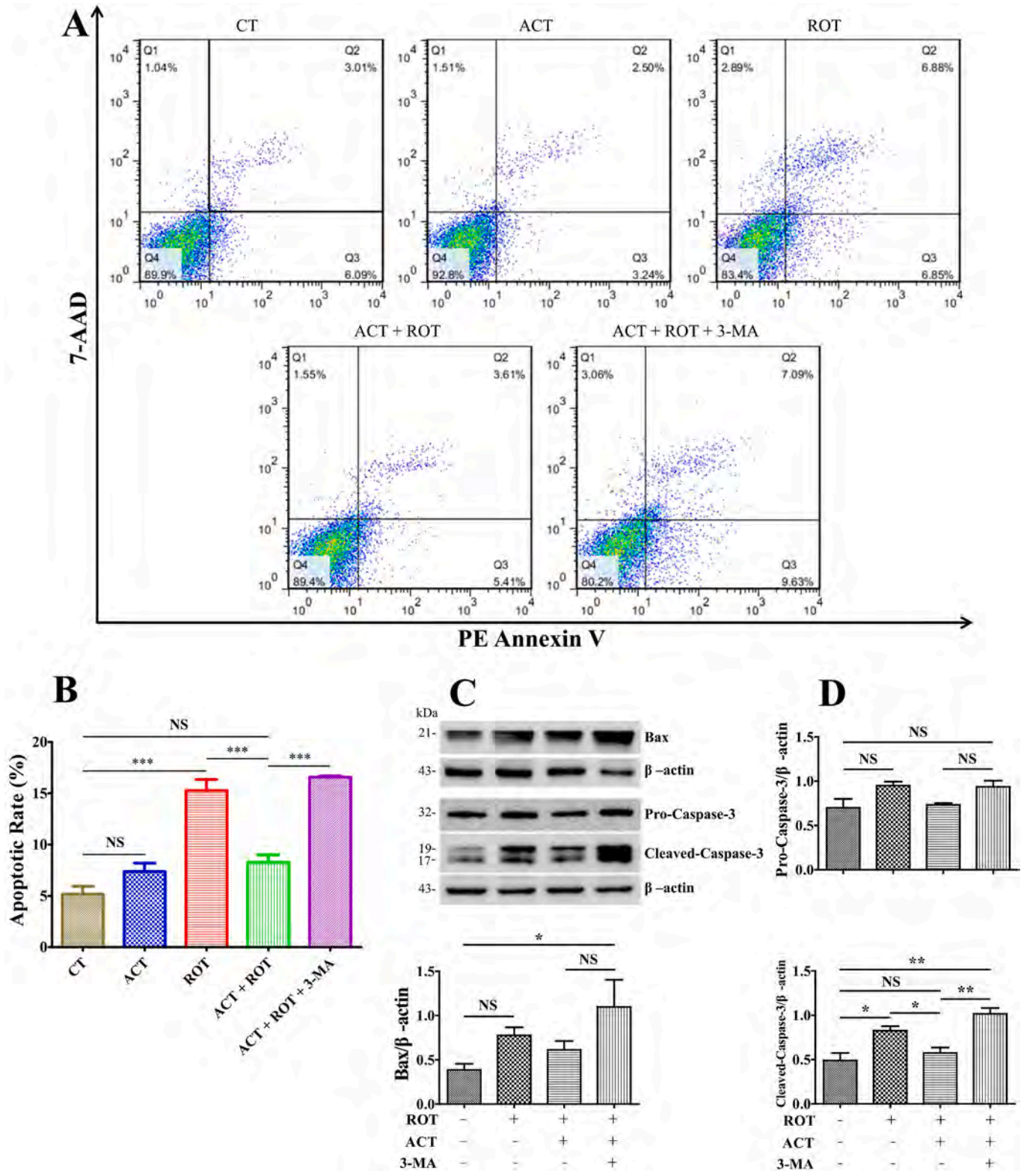

Fig. 9. ACT ameliorates ROT-induced apoptosis in PC-12 cells. (A) Cells were treated with 50 μM ACT, 0.2 μM ROT or 5 mM 3-MA as indicated for 24 h, flow cytometer analysis of apoptotic cells in PC-12 cells. (B) Ratio of apoptotic cells as shown in panel (A) was demonstrated that ACT significantly reversed the effect of ROT on PC-12 cell apoptosis, but the addition of 3-MA completely blocked the ACT's anti-apoptotic effect. Data were presented as mean ± S.E.M. of three independent experiments. (***$P < 0.01$, one-way ANOVA for multiple comparison and Newman-Keuls test as post hoc test). (C, D) Western blots analyses of Bax, Pro-Caspase-3, and Cleaved-Caspase-3 protein expression in PC-12 cells. Data were presented as mean ± S.E.M. of three or four independent experiments. (*$P < 0.05$, **$P < 0.01$, one-way ANOVA for multiple comparison and Newman-Keuls test as post hoc test).

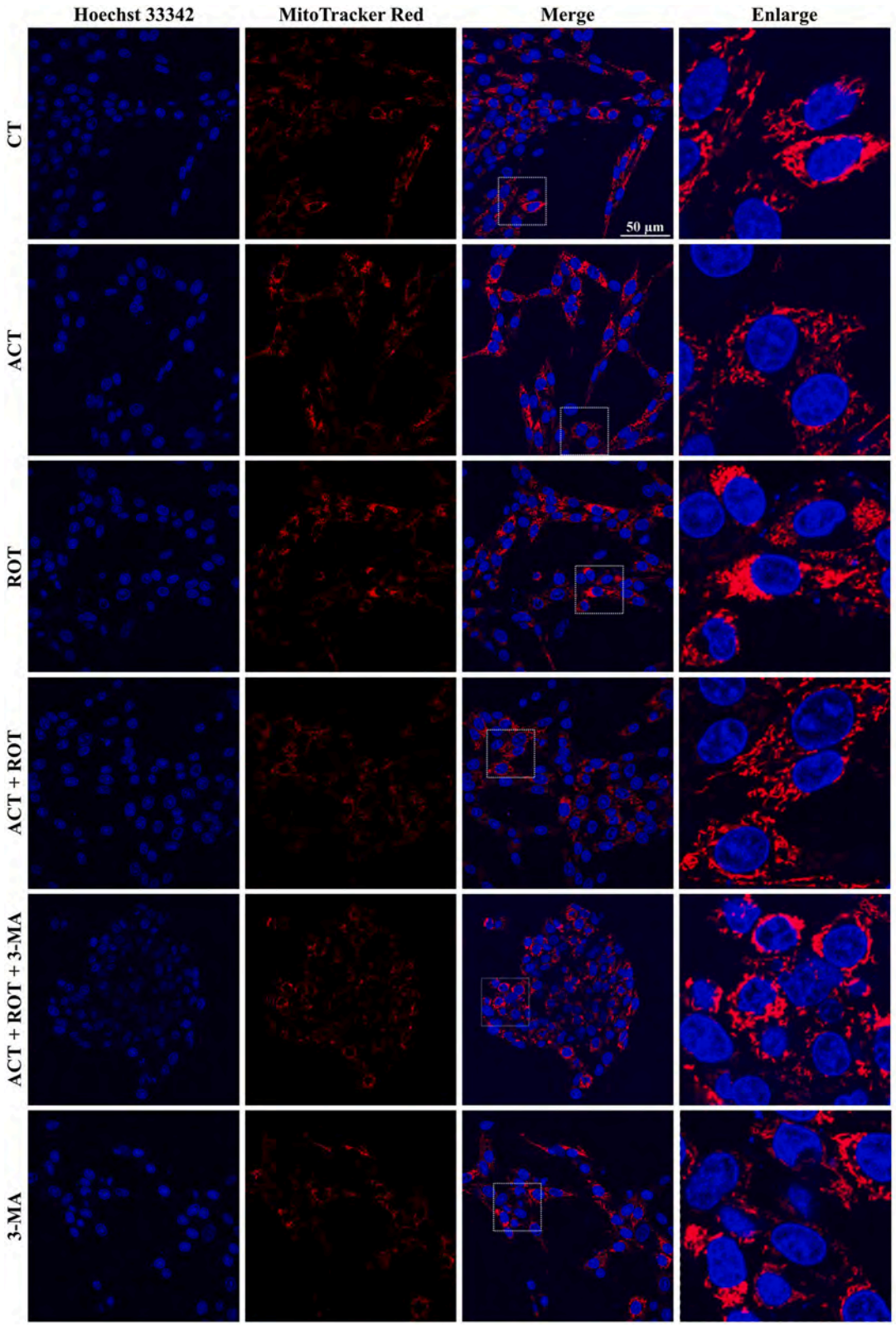

Fig. 10. ACT protects ROT -induced mitochondria injury. PC-12 cells were treated with 50 μM ACT, 0.2 μM ROT or 5 mM 3-MA as indicated for 24 h; changes in mitochondria following exposure to ROT or ACT were visualized under a laser confocal microscope. ACT remarkably ameliorated the pathological condition of ROT -induced mitochondria injury, but 3-MA completely blocked the protection effects of ACT on mitochondria.

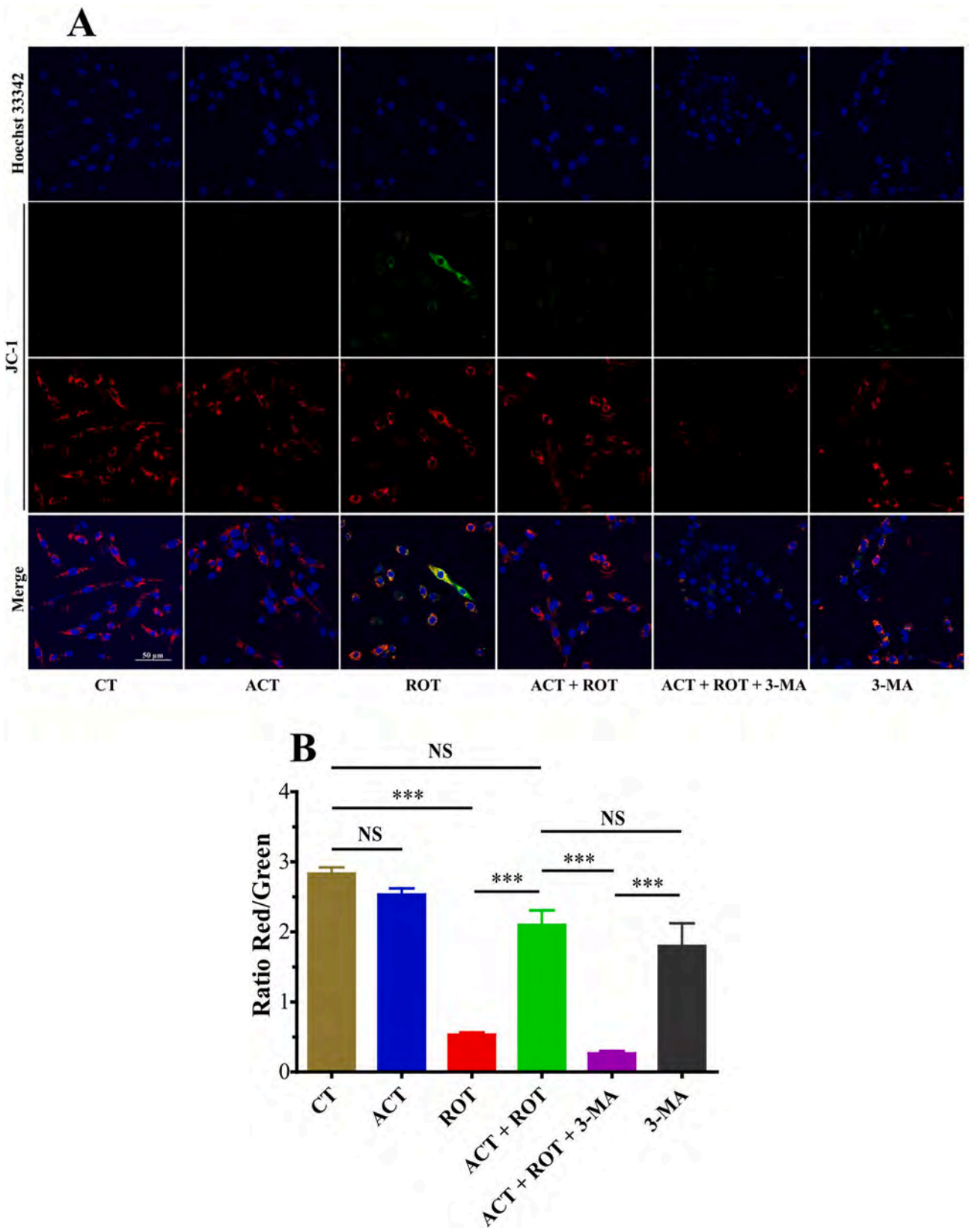

Fig. 11. ACT increases mitochondrial Δψm. (A) PC-12 cells were treated with 50 μM ACT, 0.2 μM ROT or 5 mM 3-MA as indicated for 24 h, changes in mitochondrial Δψm following exposure to ROT or ACT were determined by JC-1 staining and visualized under confocal microscope. (B) The quantification of red/green fluorescence intensity. ACT remarkably reversed the effect of ROT on PC-12 cell mitochondrial Δψm decreasing, while the addition of 3-MA completely blocked the protective effects of ACT on mitochondria function. Data were presented as mean ± S.E.M. of three independent experiments. (***$P < 0.001$, one-way ANOVA for multiple comparison and Newman-Keuls test as post hoc test).

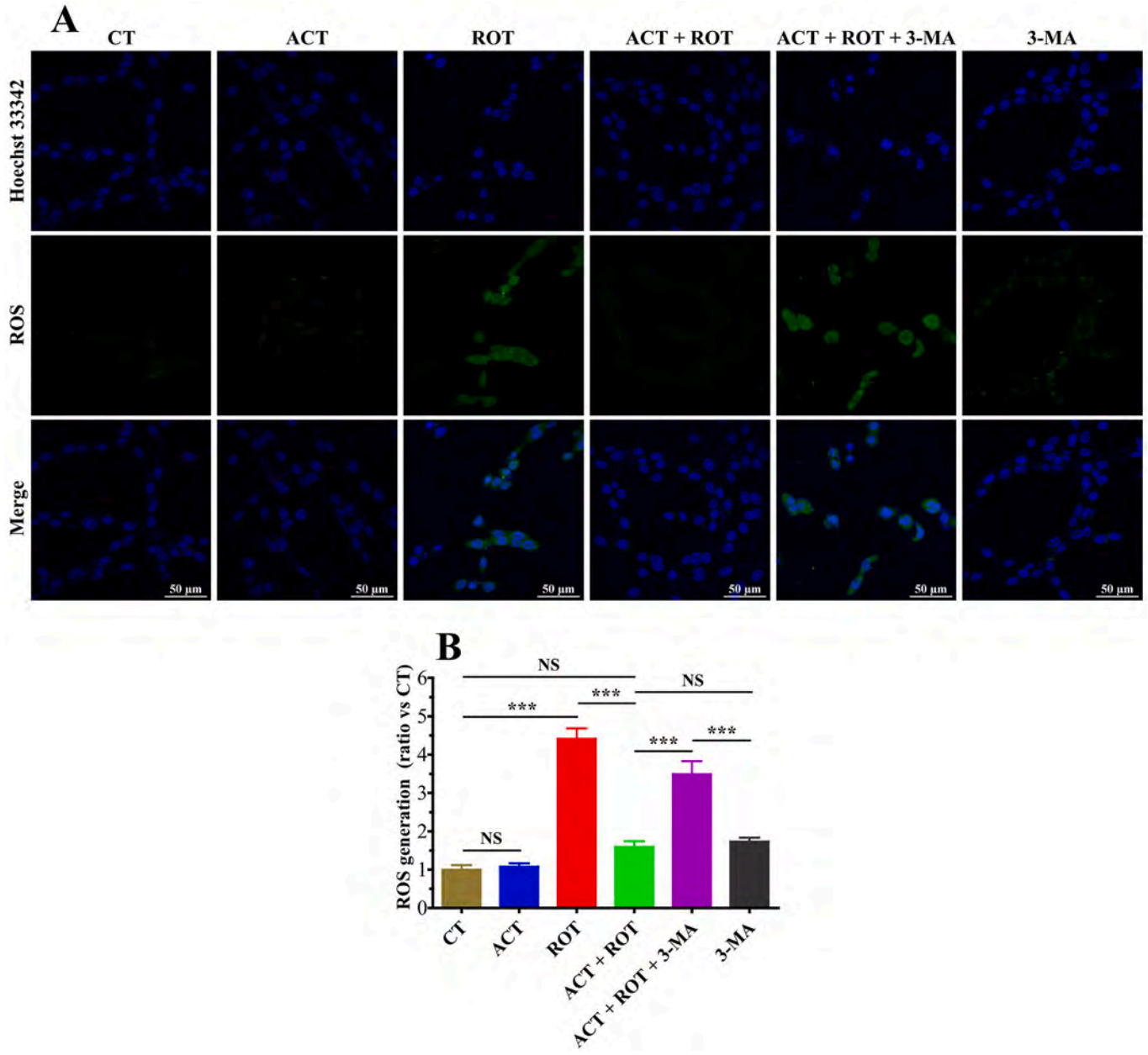

Fig. 12. ACT inhibits ROT -induced ROS production in PC-12 cells. (A) After 24 h of drug treatment, cells were stained with Hoechst 33342 and D_2CFH-DA for 30 min. ROS relevant fluorescence amount was analyzed under confocal microscope. (B) Fluorescence intensity of intracellular level of ROS generation is calculated and analyzed. ACT remarkably reversed the effect of ROT on PC-12 cell ROS generation, but the addition of 3-MA completely blocked the ACT anti-oxidation effects. Data were presented as mean ± S.E.M. of three independent experiments. (*$P < 0.05$, **$P < 0.01$, one-way ANOVA for multiple comparison and Newman-Keuls test as post hoc test).

inducers in the rodent models of neurodegenerative diseases have not been thoroughly explored yet. In future studies, transgenic animals that overexpress wild type or mutant SNCA could also be used to confirm the neuroprotective effect of ACT. We are excited to further confirm that enhancement of autophagy and mitophagy by ACT can reverse the pathological processes and relieve PD symptoms in new animal models such as rodent brain.

5. Conclusions

In our study, ACT is proven to be a safe and potent mitophagy inducer, since it did improve mitochondrial and cellular health in both PD cell model and *D. melanogaster* model. ACT decreased SNCA in appropriate level without causing cytotoxicity. The toxic effects of ROT to neuronal cells and *D. melanogaster* are prevented by the treatment with ACT. Collectively, our findings implied that ACT could be a more beneficial treatment option with no or minimal side effects for neurodegenerative diseases, especially for PD via modulating autophagy, apoptosis and other signaling pathways. To further confirm those findings, more studies needed to be done on cell models, animal models, and patients. Given that, ACT has a good security profile in international pharmaceutical knowledge base "DRUG BANK", and is currently used as an excipient in many pharmaceutical formulations for human use. We strongly believe that ACT could be a viable candidate for further development as a potential therapeutic option for patients with PD, either as a monotherapeutic or in conjunction with other therapeutic candidates.

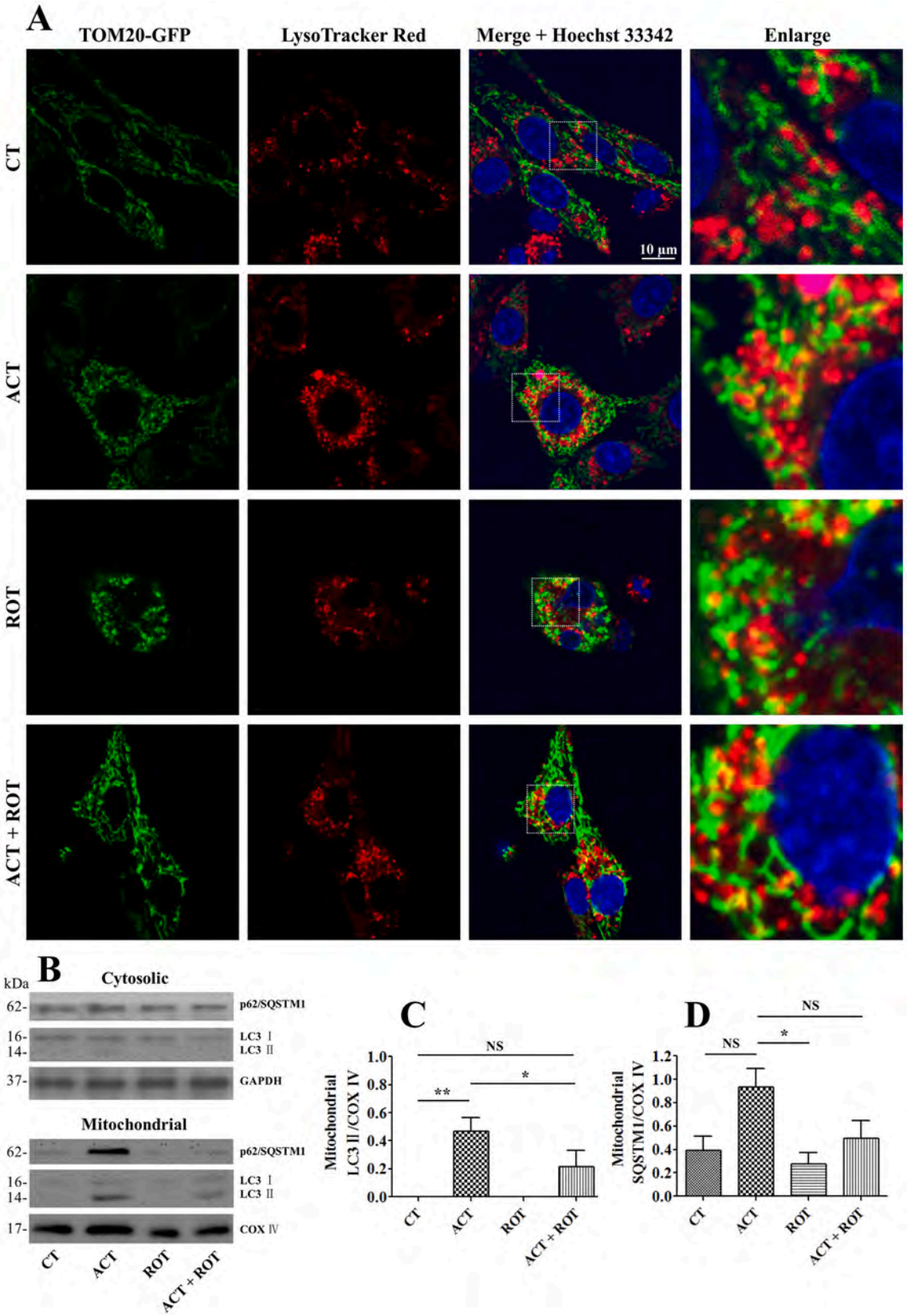

Fig. 13. ACT enhances mitophagy. (A) PC-12 cells were stably transfected with TOM20-GFP plasmid and maintained for selection by G418 for 4–5 weeks. TOM20-GFP stably expressed PC-12 cells were treated with 50 μM ACT or 0.2 μM ROT as indicated for 24 h, and subjected to confocal microscope analysis. (B) SH-SY5Y cells were treated with 50 μM ACT or 0.2 μM ROT as indicated for 24 h. Mitochondrial and cytosolic proteins were extracted and subjected to WB analysis. (C, D) Quantitative analysis of p62/SQSTM1, LC3IandII protein levels was demonstrated. Data were presented as mean ± S.E.M. of three independent experiments. (*$P <$ 0.05, **$P < 0.01$, one-way ANOVA for multiple comparison and Newman-Keuls test as post hoc test).

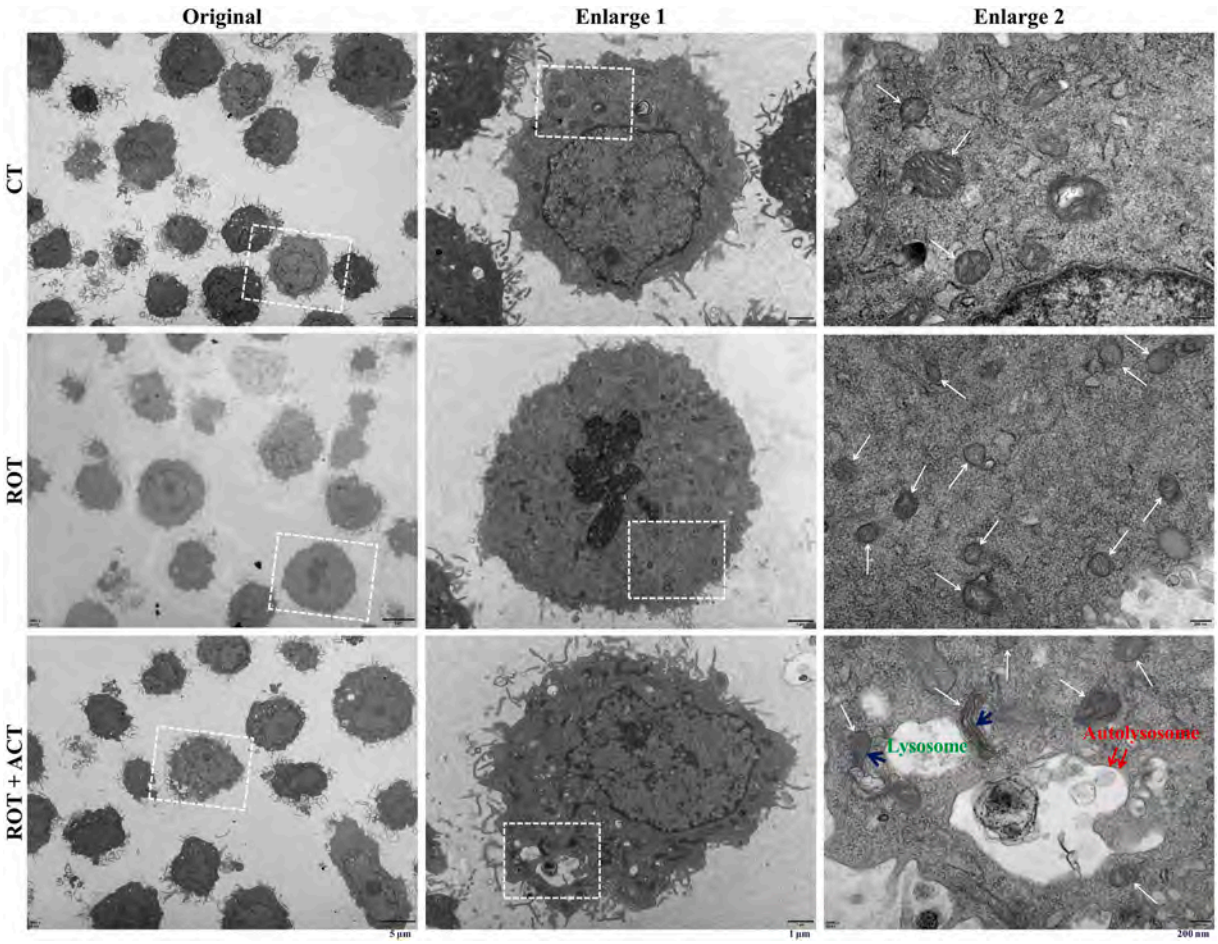

Fig. 14. ACT protects ROT -induced cell injury. PC-12 cells were treated with 50 μM ACT or 0.2 μM ROT as indicated for 16 h, changes in mitochondria following exposure to ROT or ACT were visualized under TEM. ACT treatment remarkably ameliorated the pathology of ROT -induced PC-12 cell injury. ROT treatment not only increased the rate of mitochondria fission, also increased the number of damaged mitochondria. ACT treatment selectively activated mitophagy pathway, thereby cleared damaged mitochondria (Blue Arrow - damaged mitochondrion).

Credit author statement

M.A., A.W., and N.M. participated in research design, performance of research, data analysis, and the writing of the paper. Y.A., Y.Z., X.X., Y. A., XY.L, Q.C., and XZ.F participated in performance of research, and data analysis. All authors discussed the results and approved the final manuscript.

Declaration of competing interest

None declared.

Acknowledgments

The authors would like to thank Prof. Jie Qiong Tan for providing the α-synuclein aggregated cell strains, Prof. Li Yu for providing GFP-LC3 stably expressing NRK cells and TOM20-GFP plasmids, and Dr. Shamshidin Abduriyim (College of Life Science, Shihezi University) for his writing assistance. This work was supported by the Natural Science Foundation of Xinjiang Uygur Autonomous Region (Grant No. 2017D01C213), and Department of Education, Xinjiang Uygur Autonomous Region, China (Grant No. XJEDU2021Y029).

Abbreviations

ACT Acteoside
PD Parkinson's disease
ROT rotenone
D.melanogaster *Drosophila melanogaster*
SNCA α-synuclein
DAVID database for annotation, visualization and integrated discovery
GO gene ontology
KEGG Kyoto encyclopedia of genes and genomes
GAPDH glyceraldehyde-3-phosphate dehydrogenase
MAPK mitogen activated protein-kinase
DMEM Dulbecco's Modified Eagle's Medium
PBS phosphate-buffered saline
MTT 3-[4,5-dimethylthiazol-2-yl]-2,5 diphenyl tetrazolium bromide
DMSO dimethyl sulfoxide;
PC-12 cells rat pheochromoytoma cells
SH-SY5Y cells human neuroblastoma cells
L3 larvae, third instar larvae
TEM transmission electron microscopy
NRK cells, normal rat kidney cells
HEK293 cells human embryonic kidney 293 cells
Rapa rapamycin
LC3 microtubule - associated protein light chain 3
GFP green fluorescent protein
GN-link-SNCA and SNCA-GC GFP NH_2-terminal-link-SNCA and SNCA-GFP COOH-terminal

3-MA	3-methyladenine
AMPK	5′ adenosine monophosphate activated protein kinase
mTOR	mammalian target of rapamycin
p70S6K	p70 ribosomal protein S6 kinase
HIF1	hypoxia inducible factor 1
PI3K	phosphoinositide-3-kinase
FoxO	forkhead box O
WB	Western blotting
Bax	Bcl-2 associated X protein
H_2DCF-DA	2′, 7’ -dichlorofuorescein-diacetate
ROS	reactive oxygen species
Mitochondrial Δψm	mitochondrial membrane potential
p62/SQSTM1	sequestosome 1
COX Ⅳ	cyclooxygenase Ⅳ
TOM20	translocase of the outer membrane 20
G418	geneticin
TNF	tumor necrosis factor
MMP9	matrix metallopeptidase 9
ANXA5	annexinA5
ERK	extracellular regulated protein kinases
SOD	superoxide dismutases
HMOX1Q	heme oxygenase-1
NOS3	nitric oxide synthase 3
IGF1	insulin like growth factor 1
GSK3β	glycogen synthase kinase 3β
APP	amyloid beta precursor protein
LRRK2	leucine-rich repeat kinase 2

References

An, C., Pu, X., Wang, Q., Zhang, H., 2019. Cistanche extracts ameliorates the neurotoxicity induced by hydrogen peroxide in new mutant DJ-1-transfected neuroblastoma cellular models. Brain Behav. 9 https://doi.org/10.1002/brb3.1304.

Angelopoulou, E., Paudel, Y.N., Piperi, C., 2019. miR-124 and Parkinson’s disease: a biomarker with therapeutic potential. Pharmacol. Res. 150, 104515. https://doi.org/10.1016/j.phrs.2019.104515.

Archer, S.L., 2013. Mitochondrial dynamics–mitochondrial fission and fusion in human diseases. N. Engl. J. Med. 369, 2236–2251. https://doi.org/10.1056/NEJMra1215233.

Areiza-Mazo, N., Robles, J., Zamudio-Rodriguez, J.A., Giraldez, L., Echeverria, V., Barrera-Bailon, B., Aliev, G., Sahebkar, A., Ashraf, G.M., Barreto, G.E., 2018. Extracts of physalis peruviana protect astrocytic cells under oxidative stress with rotenone. Front Chem. 6, 276. https://doi.org/10.3389/fchem.2018.00276, 276.

Biosa, A., De Lazzari, F., Masato, A., Filograna, R., Plotegher, N., Beltramini, M., Bubacco, L., Bisaglia, M., 2019. Superoxide dismutases SOD1 and SOD2 rescue the toxic effect of dopamine-derived products in human SH-SY5Y neuroblastoma cells. Neurotox. Res. 36, 746–755. https://doi.org/10.1007/s12640-019-00078-y.

Chung, S.J., Armasu, S.M., Biernacka, J.M., Lesnick, T.G., Rider, D.N., Cunningham, J. M., Maraganore, D.M., 2011. Variants in estrogen-related genes and risk of Parkinson’s disease. Mov. Disord. 26, 1234–1242. https://doi.org/10.1002/mds.23604.

Çomoğlu, S.S., Güven, H., Acar, M., Öztürk, G., Koçer, B., 2013. Tear levels of tumor necrosis factor-alpha in patients with Parkinson’s disease. Neurosci. Lett. 553, 63–67. https://doi.org/10.1016/j.neulet.2013.08.019.

Consortium, U., 2017. UniProt: the universal protein knowledgebase. Nucleic Acids Res. 45, D158–d169. https://doi.org/10.1093/nar/gkw1099.

Daina, A., Michielin, O., Zoete, V., 2019. SwissTargetPrediction: updated data and new features for efficient prediction of protein targets of small molecules. Nucleic Acids Res. 47, W357–W364. https://doi.org/10.1093/nar/gkz382.

de la Monte, S.M., Jhaveri, A., Maron, B.A., Wands, J.R., 2007. Nitric oxide synthase 3-mediated neurodegeneration after intracerebral gene delivery. J. Neuropathol. Exp. Neurol. 66, 272–283. https://doi.org/10.1097/nen.0b013e318040cfa2.

Doktór, B., Damulewicz, M., Pyza, E., 2019. Overexpression of mitochondrial ligases reverses rotenone-induced effects in a Drosophila model of Parkinson’s disease. Front. Neurosci. 13, 94. https://doi.org/10.3389/fnins.2019.00094, 94.

Dong, R.F., Zhang, B., Tai, L.W., Liu, H.M., Shi, F.K., Liu, N.N., 2018. The neuroprotective role of MiR-124-3p in a 6-hydroxydopamine-induced cell model of Parkinson’s disease via the regulation of ANAX5. J. Cell. Biochem. 119, 269–277. https://doi.org/10.1002/jcb.26170.

Dorsey, E., Sherer, T., Okun, M., Bloem, B., 2018. The emerging evidence of the Parkinson pandemic. J. Parkinsons Dis. 8 https://doi.org/10.3233/JPD-181474. S3-S8.

Fang, E.F., Hou, Y., Palikaras, K., Adriaanse, B.A., Kerr, J.S., Yang, B., Lautrup, S., Hasan-Olive, M.M., Caponio, D., Dan, X., Rocktäschel, P., Croteau, D.L., Akbari, M., Greig, N.H., Fladby, T., Nilsen, H., Cader, M.Z., Mattson, M.P., Tavernarakis, N., Bohr, V.A., 2019. Mitophagy inhibits amyloid-β and tau pathology and reverses cognitive deficits in models of Alzheimer’s disease. Nat. Neurosci. 22, 401–412. https://doi.org/10.1038/s41593-018-0332-9.

Fecto, F., Esengul, Y.T., Siddique, T., 2014. Protein recycling pathways in neurodegenerative diseases. Alzheimer’s Res. Ther. 6, 13. https://doi.org/10.1186/alzrt243.

Gargano, J.W., Martin, I., Bhandari, P., Grotewiel, M.S., 2005. Rapid iterative negative geotaxis (RING): a new method for assessing age-related locomotor decline in Drosophila. Exp. Gerontol. 40, 386–395. https://doi.org/10.1016/j.exger.2005.02.005.

Gaulton, A., Hersey, A., Nowotka, M., Bento, A.P., Chambers, J., Mendez, D., Mutowo, P., Atkinson, F., Bellis, L.J., Cibrián-Uhalte, E., Davies, M., Dedman, N., Karlsson, A., Magariños, M.P., Overington, J.P., Papadatos, G., Smit, I., Leach, A.R., 2017. The ChEMBL database in 2017. Nucleic Acids Res. 45, D945–D954. https://doi.org/10.1093/nar/gkw1074.

Gong, J., Cai, C., Liu, X., Ku, X., Jiang, H., Gao, D., Li, H., 2013. ChemMapper: a versatile web server for exploring pharmacology and chemical structure association based on molecular 3D similarity method. Bioinformatics 29, 1827–1829. https://doi.org/10.1093/bioinformatics/btt270.

Hong, C.-T., Chan, L., Hu, C.-J., Lin, C.-M., Hsu, C.-Y., Lin, M.-C., 2017. Tamoxifen and the risk of Parkinson’s disease in female patients with breast cancer in asian people: a nationwide population-based study. J. Breast Canc. 20, 356–360. https://doi.org/10.4048/jbc.2017.20.4.356.

Hou, X., Watzlawik, J.O., Fiesel, F.C., Springer, W., 2020. Autophagy in Parkinson’s disease. J. Mol. Biol. 432, 2651–2672. https://doi.org/10.1016/j.jmb.2020.01.037.

Hwang, S., Disatnik, M.-H., Mochly-Rosen, D., 2015. Impaired GAPDH-induced mitophagy contributes to the pathology of Huntington’s disease. EMBO Mol. Med. 7, 1307–1326. https://doi.org/10.15252/emmm.201505256.

Ito, K., Murphy, D., 2013. Application of ggplot2 to pharmacometric graphics. CPT Pharmacometrics Syst. Pharmacol. 2, e79. https://doi.org/10.1038/psp.2013.56 e79.

Jiang, X., Jiang, H., Shen, Z., Wang, X., 2014. Activation of mitochondrial protease OMA1 by Bax and Bak promotes cytochrome c release during apoptosis. Proc. Natl. Acad. Sci. U.S.A. 111, 14782–14787. https://doi.org/10.1073/pnas.1417253111.

Jiang, X., Li, L., Ying, Z., Pan, C., Huang, S., Li, L., Dai, M., Yan, B., Li, M., Jiang, H., Chen, S., Zhang, Z., Wang, X., 2016. A small molecule that protects the integrity of the electron transfer chain blocks the mitochondrial apoptotic pathway. Mol. Cell 63, 229–239. https://doi.org/10.1016/j.molcel.2016.06.016.

Kadigamuwa, C.C., Mapa, M.S.T., Wimalasena, K., 2016. Lipophilic cationic cyanines are potent complex I inhibitors and specific in vitro dopaminergic toxins with mechanistic similarities to both rotenone and MPP(.). Chem. Res. Toxicol. 29, 1468–1479. https://doi.org/10.1021/acs.chemrestox.6b00138.

Kandil, E.A., Sayed, R.H., Ahmed, L.A., Abd El Fattah, M.A., El-Sayeh, B.M., 2019. Hypoxia-inducible factor 1 alpha and nuclear-related receptor 1 as targets for neuroprotection by albendazole in a rat rotenone model of Parkinson’s disease. Clin. Exp. Pharmacol. Physiol. 46, 1141–1150. https://doi.org/10.1111/1440-1681.13162.

Kapoor, S., 2012. Close association between polymorphisms of the nitric oxide synthetase 3 gene and neurological disorders other than stroke. Int. J. Gen. Med. 5, 431–432. https://doi.org/10.2147/ijgm.S31983.

Kodani, A., Kikuchi, T., Tohda, C., 2019. Acteoside improves muscle atrophy and motor function by inducing new myokine secretion in chronic spinal cord injury. J. Neurotrauma 36, 1935–1948. https://doi.org/10.1089/neu.2018.6000.

Li, M., Zhou, F., Xu, T., Song, H., Lu, B., 2018. Acteoside protects against 6-OHDA-induced dopaminergic neuron damage via Nrf2-ARE signaling pathway. Food Chem. Toxicol. : Int. J. Publ. Br. Industr. Biol. Res. Assoc. 119, 6–13. https://doi.org/10.1016/j.fct.2018.06.018.

Li, W., Deng, R., Jing, X., Chen, J., Yang, D., Shen, J., 2020. Acteoside ameliorates experimental autoimmune encephalomyelitis through inhibiting peroxynitrite-mediated mitophagy activation. Free Radic. Biol. Med. 146, 79–91. https://doi.org/10.1016/j.freeradbiomed.2019.10.408.

Lim, E.W., Aarsland, D., Ffytche, D., Taddei, R.N., van Wamelen, D.J., Wan, Y.-M., Tan, E.K., Ray Chaudhuri, K., Kings Parcog group MDS Nonmotor study group, 2019. Amyloid-β and Parkinson’s disease. J. Neurol. 266, 2605–2619. https://doi.org/10.1007/s00415-018-9100-8.

Liu, J., Liu, W., Li, R., Yang, H., 2019. Mitophagy in Parkinson’s disease: from pathogenesis to treatment. Cells 8. https://doi.org/10.3390/cells8070712.

Liu, X., Ouyang, S., Yu, B., Liu, Y., Huang, K., Gong, J., Zheng, S., Li, Z., Li, H., Jiang, H., 2010. PharmMapper server: a web server for potential drug target identification using pharmacophore mapping approach. Nucleic Acids Res. 38, W609–W614. https://doi.org/10.1093/nar/gkq300.

Lu, J.H., Tan, J.Q., Durairajan, S.S., Liu, L.F., Zhang, Z.H., Ma, L., Shen, H.M., Chan, H.Y., Li, M., 2012. Isorhynchophylline, a natural alkaloid, promotes the degradation of alpha-synuclein in neuronal cells via inducing autophagy. Autophagy 8, 98–108. https://doi.org/10.4161/auto.8.1.18313.

Lu, M., Su, C., Qiao, C., Bian, Y., Ding, J., Hu, G., 2016. Metformin prevents dopaminergic neuron death in MPTP/P-induced mouse model of Parkinson’s disease via autophagy and mitochondrial ROS clearance. Int. J. Neuropsychopharmacol. 19 https://doi.org/10.1093/ijnp/pyw047.

Miller, R.L., James-Kracke, M., Sun, G.Y., Sun, A.Y., 2009. Oxidative and inflammatory pathways in Parkinson’s disease. Neurochem. Res. 34, 55–65. https://doi.org/10.1007/s11064-008-9656-2.

Nandi, A., Yan, L.J., Jana, C.K., Das, N., 2019. Role of catalase in oxidative stress- and age-associated degenerative diseases. Oxid. Med. Cell. Longev. 9613090. https://doi.org/10.1155/2019/9613090, 2019.

Neufeld, T.P., 2008. In: Chapter Thirty-Six Genetic Manipulation and Monitoring of Autophagy in Drosophila Methods in Enzymology. Academic Press, pp. 653–667. https://doi.org/10.1016/S0076-6879(08)03236-9.

Nichols, C.D., Becnel, J., Pandey, U.B., 2012. Methods to assay Drosophila behavior. JoVE : JoVE. https://doi.org/10.3791/3795.

Nitti, M., Piras, S., Brondolo, L., Marinari, U.M., Pronzato, M.A., Furfaro, A.L., 2018. Heme oxygenase 1 in the nervous system: does it favor neuronal cell survival or induce neurodegeneration? Int. J. Mol. Sci. 19 https://doi.org/10.3390/ijms19082260.

Obergasteiger, J., Frapporti, G., Pramstaller, P.P., Hicks, A.A., Volta, M., 2018. A new hypothesis for Parkinson's disease pathogenesis: GTPase-p38 MAPK signaling and autophagy as convergence points of etiology and genomics. Mol. Neurodegener. 13, 40. https://doi.org/10.1186/s13024-018-0273-5.

Oxenkrug, G.F., Navrotskaya, V., Voroboyva, L., Summergrad, P., 2011. Extension of life span of Drosophila melanogaster by the inhibitors of tryptophan-kynurenine metabolism. Fly 5, 307–309. https://doi.org/10.4161/fly.5.4.18414.

Pan, P.-Y., Zhu, Y., Shen, Y., Yue, Z., 2019. Crosstalk between presynaptic trafficking and autophagy in Parkinson's disease. Neurobiol. Dis. 122, 64–71. https://doi.org/10.1016/j.nbd.2018.04.020.

Pickles, S., Vigié, P., Youle, R.J., 2018. Mitophagy and quality control mechanisms in mitochondrial maintenance. Curr. Biol. 28, R170–R185. https://doi.org/10.1016/j.cub.2018.01.004.

Piñero, J., Bravo, À., Queralt-Rosinach, N., Gutiérrez-Sacristán, A., Deu-Pons, J., Centeno, E., García-García, J., Sanz, F., Furlong, L.I., 2017. DisGeNET: a comprehensive platform integrating information on human disease-associated genes and variants. Nucleic Acids Res. 45, D833–d839. https://doi.org/10.1093/nar/gkw943.

Piñero, J., Ramírez-Anguita, J.M., Saüch-Pitarch, J., Ronzano, F., Centeno, E., Sanz, F., Furlong, L.I., 2020. The DisGeNET knowledge platform for disease genomics: 2019 update. Nucleic Acids Res. 48, D845–D855. https://doi.org/10.1093/nar/gkz1021.

Prajapati, K.D., Sharma, S.S., Roy, N., 2011. Current perspectives on potential role of albumin in neuroprotection. Rev. Neurosci. 22, 355–363. https://doi.org/10.1515/rns.2011.028.

Probert, L., 2015. TNF and its receptors in the CNS: the essential, the desirable and the deleterious effects. Neuroscience 302, 2–22. https://doi.org/10.1016/j.neuroscience.2015.06.038.

Rempe, R.G., Hartz, A.M.S., Bauer, B., 2016. Matrix metalloproteinases in the brain and blood-brain barrier: versatile breakers and makers. J. Cerebr. Blood Flow Metabol. : Off. J. Int. Soc. Cerebral Blood Flow Metabol. 36, 1481–1507. https://doi.org/10.1177/0271678x16655551.

Rice, H.C., de Malmazet, D., Schreurs, A., Frere, S., Van Molle, I., Volkov, A.N., Creemers, E., Vertkin, I., Nys, J., Ranaivoson, F.M., Comoletti, D., Savas, J.N., Remaut, H., Balschun, D., Wierda, K.D., Slutsky, I., Farrow, K., De Strooper, B., de Wit, J., 2019. Secreted Amyloid-β Precursor Protein Functions as a GABA(B)R1a Ligand to Modulate Synaptic Transmission. Science, New York, N.Y., p. 363. https://doi.org/10.1126/science.aao4827

Rubinsztein, D.C., Gestwicki, J.E., Murphy, L.O., Klionsky, D.J., 2007. Potential therapeutic applications of autophagy. Nat. Rev. Drug Discov. 6, 304–312. https://doi.org/10.1038/nrd2272.

Rusmini, P., Cortese, K., Crippa, V., Cristofani, R., Cicardi, M.E., Ferrari, V., Vezzoli, G., Tedesco, B., Meroni, M., Messi, E., Piccolella, M., Galbiati, M., Garrè, M., Morelli, E., Vaccari, T., Poletti, A., 2019. Trehalose induces autophagy via lysosomal-mediated TFEB activation in models of motoneuron degeneration. Autophagy 15, 631–651. https://doi.org/10.1080/15548627.2018.1535292.

Scheibye-Knudsen, M., Fang, E.F., Croteau, D.L., Wilson 3rd, D.M., Bohr, V.A., 2015. Protecting the mitochondrial powerhouse. Trends Cell Biol. 25, 158–170. https://doi.org/10.1016/j.tcb.2014.11.002.

Sekar, S., Taghibiglou, C., 2020. Nuclear accumulation of GAPDH, GluA2 and p53 in post-mortem substantia nigral region of patients with Parkinson's disease. Neurosci. Lett. 716, 134641. https://doi.org/10.1016/j.neulet.2019.134641.

Sekigawa, A., Takamatsu, Y., Sekiyama, K., Takenouchi, T., Sugama, S., Waragai, M., Fujita, M., Hashimoto, M., 2013. Diversity of mitochondrial pathology in a mouse model of axonal degeneration in synucleinopathies. Oxid. Med. Cell. Longev. 817807. https://doi.org/10.1155/2013/817807, 2013.

Villa, A., Vegeto, E., Poletti, A., Maggi, A., 2016. Estrogens, neuroinflammation, and neurodegeneration. Endocr. Rev. 37, 372–402. https://doi.org/10.1210/er.2016-1007.

Xia, D., Zhang, Z., Zhao, Y., 2018. Acteoside attenuates oxidative stress and neuronal apoptosis in rats with focal cerebral ischemia-reperfusion injury. Biol. Pharm. Bull. 41, 1645–1651. https://doi.org/10.1248/bpb.b18-00210.

Xiromerisiou, G., Hadjigeorgiou, G.M., Papadimitriou, A., Katsarogiannis, E., Gourbali, V., Singleton, A.B., 2008. Association between AKT1 gene and Parkinson's disease: a protective haplotype. Neurosci. Lett. 436, 232–234. https://doi.org/10.1016/j.neulet.2008.03.026.

Yang, L., Wang, H., Liu, L., Xie, A., 2018. The role of insulin/IGF-1/PI3K/Akt/GSK3β signaling in Parkinson's disease dementia. Front. Neurosci. 12, 73. https://doi.org/10.3389/fnins.2018.00073.

Yu, G., Wang, L.-G., Han, Y., He, Q.-Y., 2012. clusterProfiler: an R Package for comparing biological themes among gene clusters. OMICS A J. Integr. Biol. 16, 284–287. https://doi.org/10.1089/omi.2011.0118.

Yuan, J., Ren, J., Wang, Y., He, X., Zhao, Y., 2016. Acteoside binds to caspase-3 and exerts neuroprotection in the rotenone rat model of Parkinson's disease. PloS One 11, e0162696. https://doi.org/10.1371/journal.pone.0162696.